

# Lawrence Berkeley National Laboratory

## LBL Publications

**Title**

On the propagation of a coupled saturation and pressure front

**Permalink**

<https://escholarship.org/uc/item/11t8n1x0>

**Journal**

Water Resources Research, 47(3)

**ISSN**

0043-1397

**Author**

Vasco, DW

**Publication Date**

2011-04-06

**DOI**

10.1029/2010WR009740

Peer reviewed

## On the propagation of a coupled saturation and pressure front

D. W. Vasco<sup>1</sup>

Received 8 July 2010; revised 8 December 2010; accepted 20 December 2010; published 25 March 2011.

[1] Using an asymptotic technique, valid for a medium with smoothly varying heterogeneity, I derive an expression for the velocity of a propagating, coupled saturation and pressure front. The asymptotic approach produces an explicit expression for the slowness, the inverse of the velocity, of a propagating two-phase front. Because of the nonlinearity of the governing equations, the velocity of the propagating front depends upon the magnitude of the saturation and pressure changes across the front in addition to the properties of the medium. Thus, the expression must be evaluated in conjunction with numerical reservoir simulation. The slowness is governed by the background saturation distribution, the saturation-dependent component of the fluid mobility, the porosity, the permeability, the capillary pressure function, the medium compressibility, and the ratio of the slopes of the relative permeability curves. Numerical simulation of water injection into a porous layer saturated with a nonaqueous phase liquid indicates that two modes of propagation are important. The fastest mode of propagation is a disturbance that is dominated by the change in fluid pressure. This is followed, much later, by a coupled mode associated with a much larger saturation change. These two modes are also observed in a numerical simulation using a heterogeneous porous layer. A comparison between the propagation times estimated from the results of the numerical simulation and predictions from the asymptotic expression indicates overall agreement.

**Citation:** Vasco, D. W. (2011), On the propagation of a coupled saturation and pressure front, *Water Resour. Res.*, 47, W03526, doi:10.1029/2010WR009740.

### 1. Introduction

[2] In a wide range of activities, including environmental remediation, the geological sequestration of carbon dioxide, and geothermal energy development, it is important to correctly model the flow of fluids within the subsurface. To this end, one must adequately characterize the flow properties at depth. This is typically accomplished through the solution of an inverse problem in which observations are used to constrain medium parameters, such as the formation permeability [Sun, 1994]. The practice of inverse modeling has advanced in recent years through improved field methods and the development of flexible modeling techniques. For example, there are networks of multilevel samplers and cross-well configurations of transducers capable of generating a dense array of observations [Hsieh *et al.*, 1985; Butler *et al.*, 1999; Karasaki *et al.*, 2000; Yeh and Liu, 2000; Veselinov *et al.*, 2001; Datta-Gupta *et al.*, 2002]. In addition, geophysical measurements have been used to augment hydrological data in order to characterize flow properties in the subsurface [Paillet, 1993; Schmidt and Bürgmann, 2003; Vasco *et al.*, 2004; Vasco, 2004b; Kowalsky *et al.*, 2004, 2005; Bell *et al.*, 2008; Vasco *et al.*, 2010; Rucci *et al.*, 2010].

[3] Given the wide variety of hydrologic and geophysical data, it is important to have access to flexible and effi-

cient approaches for modeling and inversion. Purely numerical methods provide the most comprehensive solutions to multiphase flow problems. However, numerical approaches tend to be computationally intensive and provide less insight because such solutions do not produce explicit expressions in terms of the model parameters. Analytic solutions can be efficient and do produce explicit expressions in terms of the parameters of a medium but are usually limited to fairly simple situations, such as linearized perturbations on a homogeneous background model. There are semianalytic techniques for modeling and inversion that display some of the efficiency and insight of analytic methods while extending to the more complicated situations that can be treated by numerical techniques. One class of semianalytic methods, the trajectory-based approaches described by Cohen and Lewis [1967], Shen [1983], Vasco and Datta-Gupta [1999], Vasco *et al.* [1999], and Vasco *et al.* [2000], has the additional flexibility of partitioning the inverse problem into a travel time–matching problem [Vasco and Datta-Gupta, 1999; Vasco *et al.*, 2000; Brauchler *et al.*, 2003] and an amplitude-matching problem [Vasco, 2008a]. As noted by Cheng *et al.* [2005], the travel time problem is quasi-linear and thus converges more readily than the highly nonlinear amplitude matching problem. Furthermore, inverting travel times is much more efficient than is amplitude inversion, and such inverse problems form the basis of medical imaging [Arridge, 1999] and geophysical tomography [Iyer and Hirahara, 1993].

[4] While asymptotic, trajectory-based solutions have been used to treat a number of inverse problems in hydrology [Vasco, 2008b], there are some limitations in current

<sup>1</sup>Earth Sciences Division, Lawrence Berkeley National Laboratory, University of California, Berkeley, California, USA.

derivations. Specifically, while asymptotic techniques are applicable to nonlinear processes [Whitham, 1974; Anile *et al.*, 1993] and have been applied to two-phase flow [Vasco *et al.*, 1999; Vasco, 2004a], the applications have been limited in some respects. For example, capillary effects were neglected by Vasco *et al.* [1999]. Typically, when capillary effects are included, the background fields, such as the initial saturation and the capillary pressure, are assumed to be uniform [Anile *et al.*, 1993; Vasco, 2004a]. Furthermore, when the governing equation is written in terms of a distinct saturation equation, as in the work of Vasco [2004a], the resulting equation for the velocity of the saturation front is a complicated expression that contains an implicit dependence on the solution of the pressure equation.

[5] In this paper I present a new derivation of a trajectory-based solution for two-phase flow in the presence of capillary forces. The derivation is based upon a general approach that is applicable to any set of coupled nonlinear partial differential equations. The resulting expression for the phase velocity depends explicitly upon the saturation and pressure amplitude changes in a rather simple fashion. Because of the presence of the saturation and pressure terms, the phase velocity must be calculated in conjunction with the results from a numerical simulator. However, the expression provides insight into the way in which saturation and pressure changes control the propagation of a coupled two-phase front.

## 2. Methodology

[6] In this section I present the governing equations for two-phase flow and outline an asymptotic analysis based upon the method of multiple scales. The details of that analysis are given in full in Appendix A.

### 2.1. Equations Governing Two-Phase Flow

[7] To begin, I consider the set of simultaneous partial differential equations describing the flow of a wetting phase and a nonwetting phase [Bear, 1972; Peaceman, 1977; de Marsily, 1986]:

$$\begin{aligned} \nabla \cdot \left[ \frac{\rho_w k k_{rw}}{\mu_w} \nabla (P_w - \rho_w g z) \right] &= \frac{\partial (\rho_w \phi S_w)}{\partial t}, \\ \nabla \cdot \left[ \frac{\rho_n k k_{rn}}{\mu_n} \nabla (P_n - \rho_n g z) \right] &= \frac{\partial (\rho_n \phi S_n)}{\partial t}, \end{aligned} \quad (1)$$

where  $S_w$  and  $S_n$  denote the saturation of the wetting and nonwetting phases, respectively. The relative permeabilities of the wetting and nonwetting phases, which are functions of the saturations, are represented by  $k_{rw}$  and  $k_{rn}$ , while the absolute permeability is given by  $k(\mathbf{x})$ . The respective densities are  $\rho_w$  and  $\rho_n$ , the gravitational constant is  $g$ , and the porosity is  $\phi(\mathbf{x}, t)$ . The pressure associated with the wetting phase is  $P_w(\mathbf{x}, t)$  while the nonwetting phase pressure is  $P_n(\mathbf{x}, t)$ ; the fluid viscosities are  $\mu_w$  and  $\mu_n$ . The two equations are coupled because the two fluids are assumed to fill the available pore space, and thus, their saturations sum to unity:

$$S_w + S_n = 1. \quad (2)$$

[8] I also assume that the phases are incompressible so that their densities are constant. I define the saturation-

dependent component of the fluid mobility [Peaceman, 1977, p. 18] by the ratios

$$\eta_w = \frac{k_{rw}}{\mu_w} \quad (3)$$

$$\eta_n = \frac{k_{rn}}{\mu_n}. \quad (4)$$

[9] I shall assume that the relative permeability properties are constant for a given formation. Thus, within a given heterogeneous layer I shall assume that the relative permeabilities are only functions of the fluid saturations. Because the saturations sum to unity, I can write the governing equations (1) in terms of one of the saturations, say

$$S = S_w = 1 - S_n, \quad (5)$$

and hence, the system of equations reduces to two equations in three unknowns ( $S$ ,  $P_w$ , and  $P_n$ ).

[10] To reduce the system (1) to two equations in two unknowns, I invoke the assumption that the fluid pressure difference, the capillary pressure  $P_c$ , in the pores is a function of the fluid saturation [Bear, 1972]; thus,

$$P_c(S) = P_n - P_w. \quad (6)$$

[11] As was done for the relative permeabilities, I shall assume that the capillary pressure function only varies across a layer boundary and does not depend explicitly upon the spatial location within a particular formation. Rather, in a given formation, the capillary pressure function is only a function of the pressure in one fluid phase and the saturation distribution within the layer. Denoting the fluid pressure in the wetting phase by  $P$ ,

$$P = P_w, \quad (7)$$

and writing the fluid pressure for the nonwetting phase as

$$P_n = P + P_c, \quad (8)$$

[12] I can reduce the system of equations (1) to two equations in two unknowns. First, because of equation (8), I write the gradient of the fluid pressure of the nonwetting phase in terms of the gradients of the pressure and saturation of the wetting phase:

$$\nabla P_n = \nabla P + \frac{\partial P_c}{\partial S} \nabla S. \quad (9)$$

[13] As done by de Marsily [1986], I assume linear elastic behavior for the porous matrix to arrive at a relationship between a change in fluid pressure and a change in matrix porosity. The exact relationship is

$$\frac{\partial \phi}{\partial t} = \alpha_T \frac{\partial P_w}{\partial t}, \quad (10)$$

where  $\alpha_T$  is a proportionality coefficient that depends upon the compressibilities of the fluids and the solid and on the

porosity. Making the various substitutions described above, the original system of equations (1) reduces to two equations in two unknowns:

$$\nabla \cdot [k\eta_w(\nabla P - \rho_w \mathbf{Z})] = \alpha_T S \frac{\partial P}{\partial t} + \varphi \frac{\partial S}{\partial t} \quad (11)$$

$$\nabla \cdot [k\eta_n(\nabla P + \gamma_c \nabla S - \rho_n \mathbf{Z})] = \alpha_T (1 - S) \frac{\partial P}{\partial t} - \varphi \frac{\partial S}{\partial t}, \quad (12)$$

where  $\mathbf{Z} = g\nabla z$  is a vector in the direction of the gravitational attraction and

$$\gamma_c = \frac{\partial P_c}{\partial S}. \quad (13)$$

[14] Carrying out the differentiations associated with the outer divergence operator, I can write equations (11) and (12) as the pair of equations

$$\begin{aligned} \nabla \kappa \cdot \nabla P + \chi_w \nabla S \cdot \nabla P + \nabla \cdot \nabla P - \rho_w \nabla \kappa \cdot \mathbf{Z} - \rho_w \chi_w \nabla S \cdot \mathbf{Z} \\ = \frac{\alpha_T}{k\eta_w} S \frac{\partial P}{\partial t} + \frac{\phi}{k\eta_w} \frac{\partial S}{\partial t} \end{aligned} \quad (14)$$

$$\begin{aligned} \nabla \kappa \cdot \nabla P + \chi_n \nabla S \cdot \nabla P + \nabla \cdot \nabla P - \rho_n \nabla \kappa \cdot \mathbf{Z} - \rho_n \chi_n \nabla S \cdot \mathbf{Z} \\ + \gamma_c \nabla \kappa \cdot \nabla S + \Upsilon \nabla S \cdot \nabla S + \gamma_c \nabla \cdot \nabla S \\ = \frac{\alpha_T}{k\eta_n} (1 - S) \frac{\partial P}{\partial t} - \frac{\phi}{k\eta_n} \frac{\partial S}{\partial t}, \end{aligned} \quad (15)$$

where

$$\kappa = -\ln k, \quad (16)$$

$$\chi_w = -\frac{\partial \eta_w}{\partial S}, \quad (17)$$

$$\chi_n = -\frac{\partial \eta_n}{\partial S}, \quad (18)$$

$$\Upsilon = \gamma_c \chi_n + \frac{\partial \gamma_c}{\partial S}. \quad (19)$$

[15] Equations (14) and (15) are the governing equations and serve as the starting point for my application of the method of multiple scales, an asymptotic technique described in section 2.2.

## 2.2. An Asymptotic Analysis of the Governing Equations

[16] The governing equations (14) and (15) are rather complicated as they are nonlinear, of mixed character, and coupled partial differential equations with spatially varying coefficients. Without some manner of simplification an analytic solution is certainly not possible. Because one goal of this work is to develop techniques to solve inverse problems, for example, using the saturation front arrival time to infer the flow properties of the medium, retaining the heterogeneity is essential. However, because of the limited reso-

lution of most inverse methods, in which a finite number of data are used to estimate a field of properties, one typically seeks models with smoothly varying heterogeneity. Thus, I am most interested in two-phase flow in a model with smoothly varying properties. I should note that sharp boundaries, in the form of layering, are allowed as explicit boundary conditions.

[17] I can build the assumption of smoothly varying heterogeneity into the modeling through a technique known as the method of multiple scales [Anile *et al.*, 1993, p. 49]. This approach is suited to the construction of asymptotic solutions for a porous medium with heterogeneous, yet smoothly varying, flow properties. The measure of smoothness is with respect to the scale length of the two-phase front. In order to define this formally, I first denote the scale length of the two-phase front, the distance over which the saturation changes from the background value to the value behind the front, by  $l$ . In addition, let  $L$  denote the scale length of the heterogeneity within the medium. The smoothness of the medium is stipulated by the requirement that  $L \gg l$ . An asymptotic solution can be formulated in terms of the ratio of scale lengths  $\varepsilon = l/L$ . To this end, I will define the slow spatial coordinates

$$\mathbf{X} = \varepsilon \mathbf{x}, \quad (20)$$

the scale over which many of the quantities of interest, such as the travel time, will vary. Similarly, I can define a slow time:

$$T = \varepsilon t. \quad (21)$$

[18] An asymptotic solution is a power series representation of the dependent variables, that is, the saturation and pressure. The power series is in terms of the scale variable  $\varepsilon$ . For example, the saturation is represented as

$$S(\mathbf{X}, T, \theta_s) = S_b(\mathbf{X}, T) + \int_0^T e^{\theta_s(\mathbf{X}, u)} \sum_{i=0}^{\infty} \varepsilon^i S_i(\mathbf{X}, u) du, \quad (22)$$

where  $S_b$  is the background saturation that may be a function of space and time,  $\theta_s(\mathbf{X}, T)$  is a phase function that is related to the propagation time of the saturation front, and  $S_i(\mathbf{X}, T)$  is the  $i$ th contribution to the saturation amplitude. The integral appears in the representation because I will be considering a step function source, rather than a pulse-like source. The saturation contains both an explicit and an implicit dependence upon the spatial and temporal coordinates. The implicit dependence is through the phase function  $\theta_s(\mathbf{X}, T)$ . The representation (22) is in the form of a traveling front, a propagating change in the saturation with respect to the background saturation.

[19] The increase in pressure across the two-phase front has a similar representation:

$$P(\mathbf{X}, T, \theta_p) = P_b(\mathbf{X}, T) + \int_0^T e^{\theta_p(\mathbf{X}, u)} \sum_{i=0}^{\infty} \varepsilon^i P_i(\mathbf{X}, u) du. \quad (23)$$

[20] Note that the phase function for the pressure can differ from the saturation phase, meaning that the saturation and pressure can move with different speeds. This allows

the jump in pressure to propagate much faster than the saturation change, for example. In section 2.3 I will examine the situation in which  $\theta_s = \theta_p$ .

[21] The governing equations (14) and (15) can be rewritten in terms of the slow coordinates. In order to do this I first express the partial derivatives in terms of  $X_i$ ,  $T$ , and  $\theta$ . In doing so I make use of the relationships (20) and (21) between the fast and slow coordinates and the explicit and implicit dependence upon the independent variables. Thus, I can write the partial derivative with respect to time as

$$\frac{\partial S}{\partial t} = \varepsilon \frac{\partial S}{\partial T} + \frac{\partial \theta_s}{\partial t} \frac{\partial S}{\partial \theta_s} \quad (24)$$

because, from the definition of  $T$  in equation (21),  $\partial T / \partial t = \varepsilon$ . Similarly, I can express the derivative with respect to  $x_i$  as

$$\frac{\partial S}{\partial x_i} = \varepsilon \frac{\partial S}{\partial X_i} + \frac{\partial \theta_s}{\partial x_i} \frac{\partial S}{\partial \theta_s}, \quad (25)$$

and thus, the gradient in terms of the  $\mathbf{X}$  coordinates is given by

$$\nabla_X S = \varepsilon \nabla_X S + \nabla_{\theta_s} \frac{\partial S}{\partial \theta_s}, \quad (26)$$

where the subscripts  $X$  and  $x$  indicate that the derivatives are with respect to the  $\mathbf{X}$  and  $\mathbf{x}$  coordinates, respectively.

[22] Given these expressions for the differential operators, I can rewrite the governing equations in terms of the slow variables  $\mathbf{X}$  and  $T$ . Each term will contain a factor that is the scale parameter  $\varepsilon$  raised to some power. Because I am assuming that the saturation and pressure fronts vary over a scale length that is much less than that of the heterogeneity,  $\varepsilon$  is assumed to be much smaller than unity. Therefore, terms of low order in  $\varepsilon$  will dominate in the governing equations. In Appendix A, I write the governing equations in terms of the slow variables and retain terms of lowest order in  $\varepsilon$ . In order to derive an expression for the travel time of the capillary front, I only consider terms of order  $\varepsilon^0$ . To order  $\varepsilon^0$  the governing equations take the form (see Appendix A for a complete treatment)

$$\chi_w \mathbf{s} \cdot \mathbf{p} \bar{S} \bar{P} + p^2 \bar{P} - \rho_w \chi_w \mathbf{s} \cdot \mathbf{Z} \bar{S} = \frac{\alpha_T}{k \eta_w} \bar{S} \bar{P} \frac{\partial \theta_p}{\partial t} + \frac{\varphi}{k \eta_w} \bar{S} \frac{\partial \theta_s}{\partial t} \quad (27)$$

$$\begin{aligned} & \chi_n \mathbf{s} \cdot \mathbf{p} \bar{S} \bar{P} + p^2 \bar{P} + \rho_n \chi_n \mathbf{s} \cdot \mathbf{Z} \bar{S} + \Upsilon s^2 \bar{S}^2 + \gamma_c s^2 \bar{S} \\ & = \frac{\alpha_T}{k \eta_n} (1 - S) \bar{P} \frac{\partial \theta_p}{\partial t} - \frac{\phi}{k \eta_n} \bar{S} \frac{\partial \theta_s}{\partial t}, \end{aligned} \quad (28)$$

where I have defined the gradient vectors of the phase functions  $\theta_p$  and  $\theta_s$ ,

$$\mathbf{p} = \nabla \theta_p \quad (29)$$

$$\mathbf{s} = \nabla \theta_s, \quad (30)$$

with magnitudes  $s = |\mathbf{s}| = \sqrt{\mathbf{s} \cdot \mathbf{s}}$  and  $p = |\mathbf{p}| = \sqrt{\mathbf{p} \cdot \mathbf{p}}$ , respectively. The variables  $p$  and  $s$  are known as the slowness of the propagating two-phase front because they can

be shown to be equal to the inverse of the front velocity [Kravtsov and Orlov, 1990]. The quantities  $\bar{S}$  and  $\bar{P}$ , defined by

$$\bar{S} = S_0 - S_b, \quad (31)$$

$$\bar{P} = P_0 - P_b, \quad (32)$$

signify the change in saturation and pressure from the background values to new values because of the passage of the two-phase front.

### 2.3. Expression Governing the Evolution of the Two-Phase Front

[23] The two equations (27) and (28) provide relationships between the gradients of the phase functions,  $\mathbf{s}$  and  $\mathbf{p}$ , and the amplitudes of the saturation and pressure changes,  $\bar{S}$  and  $\bar{P}$ , across the front. In this section I use equations (27) and (28) to derive explicit expressions for the magnitude of the slowness vectors  $s$  and/or  $p$  in terms of the medium and fluid properties and the amplitude changes  $\bar{S}$  and  $\bar{P}$ . The quantity  $s$  is the front slowness, the inverse of the front velocity, an important quantity for calculating the travel time of the two-phase front.

[24] However, before delving into a detailed derivation, I need to discuss an important issue regarding the nature of the propagating front. As noted, it is assumed that the leading edge of the front is defined by a rapid change in saturation and pressure. Ahead of the front, the saturation and pressure are at their background values; behind the front the saturation and/or pressure assume new values, different from the background values. The concept of a propagating front has proven extremely useful in a wide variety of fields, such as electromagnetics [Kline and Kay, 1965; Luneburg, 1966], and is central to treatments of nonlinear wave propagation [Whitham, 1974; Maslov and Omel'yanov, 2001]. Many of the coefficients, for example,  $\chi_w$ ,  $\gamma_c$ , and  $\Upsilon$ , in equations (27) and (28) are functions of the saturation and pressure. Thus, one may ask, What values of saturation and pressure should be used in determining the coefficients? Because I am interested in the arrival time of the leading edge of the front, which evolves according to the saturation and pressure encountered before the jump to new values, I will use the background conditions to compute the coefficients in (27) and (28). Following Anile *et al.* [1993], a more formal mathematical approach may be taken, on the basis of an expansion of the coefficients in powers of  $\varepsilon$ . The expansion follows from the representation of the pressure as an asymptotic series in  $\varepsilon$  (see equation (23)). Consider, for example,  $\chi_w(P)$ , which may be expanded as

$$\chi_w(P) = \chi_w(P_b + \bar{P}_0) + \varepsilon \frac{\partial \chi_w}{\partial P}(P_b + \bar{P}_0) + O(\varepsilon^2), \quad (33)$$

where

$$\bar{P}_0(\mathbf{X}, T) = \int_0^T e^{\theta(\mathbf{X}, \tau)} P_0(\mathbf{X}, \tau) d\tau \quad (34)$$

in the case of a step function source. To order  $\varepsilon$  one finds that  $\chi_w(P) = \chi_w(P_b + \bar{P}_0)$ . The moment at which the

coupled front arrives at an observation point  $\mathbf{X}$ , which I denote by  $T_{\text{arrival}}$ , the quantity  $\bar{P}_0(\mathbf{x}, T_{\text{arrival}})$  is zero, and hence,  $\chi_w(P) = \chi_w(P_b)$ .

[25] Fixing the coefficients in equations (27) and (28) to their background values, the next task involves estimating the slowness of the propagating front. If the governing equations were linear differential equations, then the zeroth-order terms would form a linear system, and one could use the condition that the linear system has a nontrivial solution to find the admissible slowness values [Kline and Kay, 1965; Kravtsov and Orlov, 1990]. Equations (27) and (28) are not linear in  $\bar{S}$  and  $\bar{P}$ ; rather, they comprise two quadratic equations. A formal approach, similar to that used for linear systems of equations [Noble and Daniel, 1977], may be based on techniques from algebraic geometry [Cox et al., 1998]. The condition under which the two polynomial equations (27) and (28) have common zeros is the vanishing of the resultant [Cox et al., 1998; Sturmfels, 2002]. The resultant is a polynomial equation in  $s$ ,  $p$  with coefficients that depend upon either  $\bar{S}$  or  $\bar{P}$  and the properties of the medium.

[26] Here I take a direct approach, first solving equation (27) for the product term,

$$\mathbf{s} \cdot \mathbf{p} \bar{S} \bar{P} = \frac{1}{\chi_w} \left( \frac{\alpha_T}{k \eta_w} S_b \bar{P} + \frac{\varphi}{k \eta_w} \bar{S} - p^2 \bar{P} - \rho_w \chi_w \mathbf{s} \cdot \mathbf{Z} \bar{S} \right), \quad (35)$$

where I have used the background value  $S_b$  for the saturation. Substituting this expression for  $\mathbf{s} \cdot \mathbf{p} \bar{S} \bar{P}$  into equation (28) and grouping terms according to their degrees in  $s$  and  $p$  gives

$$\begin{aligned} & (\Upsilon \bar{S} + \gamma_c) \bar{S} s^2 + \left( 1 - \frac{\chi_n}{\chi_w} \right) \bar{P} p^2 + \chi_n \mathbf{s} \cdot \mathbf{Z} (\rho_n - \rho_w) \bar{S} s \\ & - \frac{\alpha_T}{k} \left( \frac{1 - S_b}{\eta_n} - \frac{\chi_n S_b}{\chi_w \eta_w} \right) \bar{P} \frac{\partial \theta_p}{\partial t} + \frac{\phi}{k} \left( \frac{\chi_n}{\chi_w \eta_w} + \frac{1}{\eta_n} \right) \bar{S} \frac{\partial \theta_s}{\partial t} \quad (36) \\ & = 0, \end{aligned}$$

an equation for the slownesses.

[27] In the most general situation, in which no assumptions are made regarding  $\mathbf{s}$  and  $\mathbf{p}$ , there are more unknowns than equations. However, I am primarily interested in the propagation of a two-phase front in which the change in saturation and the change in pressure are coupled. That is, the jumps in saturation and pressure occur simultaneously as the front passes. Thus,  $\theta_s$  and  $\theta_p$ , the phase terms associated with the saturation and pressure changes, are equal to  $\theta_s = \theta_p = \theta$ ,  $\nabla \theta_s = \mathbf{s} = \mathbf{p} = \nabla \theta_p$ , and  $s = p$ . In that case, equation (36) reduces to a single quadratic equation in  $p$ :

$$\begin{aligned} & \left[ \left( 1 - \frac{\chi_n}{\chi_w} \right) \bar{P} + (\Upsilon \bar{S} + \gamma_c) \bar{S} \right] p^2 + \chi_n \mathbf{p} \cdot \mathbf{Z} (\rho_n - \rho_w) \bar{S} p \\ & - \left[ \frac{\alpha_T}{k} \left( \frac{1 - S_b}{\eta_n} - \frac{\chi_n S_b}{\chi_w \eta_w} \right) \bar{P} + \frac{\phi}{k} \left( \frac{\chi_n}{\chi_w \eta_w} + \frac{1}{\eta_n} \right) \bar{S} \right] \frac{\partial \theta}{\partial t} \quad (37) \\ & = 0. \end{aligned}$$

[28] Defining the ratio

$$\chi = \frac{\chi_n}{\chi_w} \quad (38)$$

and the coefficients

$$\Gamma = \frac{\chi_n (\rho_n - \rho_w) \bar{S}}{(1 - \chi) \bar{P} + (\Upsilon \bar{S} + \gamma_c) \bar{S}} \quad (39)$$

$$\Omega = \frac{\alpha_T [(1 - S_b) \eta_n^{-1} - \chi S_b \eta_w^{-1}] \bar{P} - \varphi [\chi \eta_w^{-1} + \eta_n^{-1}] \bar{S}}{k [(1 - \chi) \bar{P} + (\Upsilon \bar{S} + \gamma_c) \bar{S}]}, \quad (40)$$

[29] I can write equation (37) as

$$p^2 + \Gamma g \cos(\zeta) p - \Omega \frac{\partial \theta}{\partial t} = 0, \quad (41)$$

where I have used the fact that  $\mathbf{p} \cdot \mathbf{Z} = g \cos \zeta$ . The quantity  $\zeta$  signifies the angle between the slowness vector  $\mathbf{p}$  and the direction of the gravitational attraction  $\mathbf{Z}$ . As shown in section 2.4, this expression can be used in conjunction with a numerical reservoir simulator to compute the slowness and, hence, the velocity of the propagating two-phase front. In particular, one can use a numerical simulator to calculate the saturation and pressure changes over the region of interest because of the passage of the two-phase front. Thus, one obtains estimates of  $\bar{S}$  and  $\bar{P}$  which may be substituted into the expressions (39) and (40). Equation (41) for the slowness is fairly general, allowing for capillary effects as well as gravitational forces.

## 2.4. Computation of the Phase Function

[30] Recalling the definition of the phase gradient vector  $\mathbf{p}$ , given by (29), one observes that equation (41) is a differential equation for the phase function  $\theta(\mathbf{X}, t)$ :

$$\nabla \theta \cdot \nabla \theta + \Gamma \nabla \theta \cdot \mathbf{Z} - \Omega \frac{\partial \theta}{\partial t} = 0. \quad (42)$$

[31] Equation (42) is an example of a class of equations that are of fundamental importance in many areas of physics [Lanczos, 1986]. Such equations have a well-developed mathematical foundation [Courant and Hilbert, 1962; Sneddon, 2006, p. 81] that underlies ray methods in electromagnetic [Kline and Kay, 1965; Luneburg, 1966] and elastic [Karal and Keller, 1959; Kravtsov and Orlov, 1990] wave propagation.

### 2.4.1. Direct Numerical Integration

[32] The most direct method for solving equation (42) is a numerical approach, based upon finite differences. Such methods, which have grown in popularity since their inception [Crandall and Lions, 1983; Crandall et al., 1984; Vidale, 1988; Sethian, 1990; van Trier and Symes, 1991], are now well developed [Sethian, 1999]. Techniques, such as the fast marching method and level set methods [Sethian, 1999] are general and applicable to equations such as (42). The gravitational term results in preferential movement in the direction of  $\mathbf{Z}$ . However, this does not present a fundamental difficulty because there are a number of implementations of finite difference-based algorithms for propagation in an anisotropic medium [Sethian and Strain, 1992; Lecomte, 1993; Eaton, 1993; Qian and Symes, 2001; Soukina et al., 2003].

### 2.4.2. Method of Characteristics

[33] The classical alternative to a finite difference approach is to solve equation (42) using the method of

characteristics [Courant and Hilbert, 1962, p. 63]. As shown here, such an approach leads to a trajectory-based solution and an alternative numerical technique. I first write equation (42) in the form

$$\frac{\partial \theta}{\partial t} - H(\mathbf{x}, t, \mathbf{p}, \theta) = 0, \quad (43)$$

where  $H(\mathbf{x}, t, \mathbf{p}, \theta)$  is the Hamiltonian function, given by

$$H(\mathbf{x}, t, \mathbf{p}, \theta) = \Omega^{-1} \mathbf{p} \cdot \mathbf{p} + \Psi \mathbf{p} \cdot \mathbf{Z} \quad (44)$$

$$\Psi(\mathbf{x}, t, \theta) = \Omega^{-1}(\mathbf{x}, t, \theta) \Gamma(\mathbf{x}, t, \theta). \quad (45)$$

[34] The characteristic equations corresponding to the scalar partial differential equation (43) are a set of ordinary differential equations

$$\frac{dx_i}{dt} = \frac{\partial H}{\partial p_i} \quad (46)$$

$$\frac{dp_i}{dt} = -\frac{\partial H}{\partial x_i} - \frac{\partial H}{\partial \theta} p_i \quad (47)$$

that follow from geometrical arguments [Courant and Hilbert, 1962, p. 106]. The system of ordinary equations may be solved numerically, using techniques for two-point boundary value problems [Press et al., 1992, p. 745]. Note that the two sets of equations (46) and (47) display preferential flow in the  $\mathbf{Z}$  direction because of gravitational forces. This preferential flow introduces an anisotropy and modifies the trajectories. The situation is similar to that of wave propagation in an anisotropic medium and has been treated in studies of wave propagation in an anisotropic Earth [Cerveny, 1972; Chapman and Pratt, 1992].

[35] Note that if gravity is not important, for example, if the densities are close in value or if the flow is restricted to a narrow horizontal layer, equations (46) and (47) still apply; however,  $\Psi$  will vanish. Therefore, the flow will be controlled by  $\Omega$ , and there will be no preferential flow in the  $\mathbf{Z}$  direction. In that case it is possible, under certain circumstances, to write the phase function in a separable form, such as  $\theta(\mathbf{x}, t) = \beta(t)\sigma^2(\mathbf{x})$ . In Appendix B I derive an explicit expression for  $\theta(\mathbf{x}, t)$  for the case in which the phase is a separable function. In Appendix B, it is shown that

$$\beta(t) = -\frac{1}{4t} \quad (48)$$

$$\sigma(\mathbf{x}) = \int_{\mathbf{x}} \sqrt{\Omega} ds, \quad (49)$$

resulting in

$$\theta[\mathbf{x}(s), t] = -\frac{1}{4t} \left( \int_{\mathbf{x}(s)} \sqrt{\Omega} ds \right)^2, \quad (50)$$

which is similar to the phase function for the linear diffusion equation [Vasco et al., 2000].

## 2.5. Zeroth-Order Solution for the Saturation and Pressure Changes

[36] Armed with expressions for the trajectory of the propagating front and the phase function  $\theta(\mathbf{x}, t)$ , one can construct a low-order representation of the saturation and pressure fields using the series solutions (22) and (23). Because I am interested in solutions for a model with smoothly varying flow properties,  $\varepsilon$  is assumed to be small, and thus, the first few terms of the series dominate. Here I consider a zeroth-order solution, taking only the first term of each series. The expression for the saturation change with respect to the background value  $S_b(\mathbf{X}, T)$  is

$$\bar{S}(\mathbf{X}, T, \theta_s) = \int_0^T e^{\theta_s(\mathbf{X}, u)} S_0(\mathbf{X}, u) du, \quad (51)$$

and similarly for the pressure change, it is

$$\bar{P}(\mathbf{X}, T, \theta_p) = \int_0^T e^{\theta_p(\mathbf{X}, u)} P_0(\mathbf{X}, u) du. \quad (52)$$

[37] Note that these solutions are incomplete because they depend upon the amplitudes  $S_0$  and  $P_0$ , which are not provided. In fact, the defining equation for the phase, equation (42), contains coefficients  $\Gamma$  and  $\Omega$  that depend upon the amplitude changes  $\bar{S}$  and  $\bar{P}$ . Thus, expression (51) and (52) must be evaluated in conjunction with estimates of the amplitude changes  $S_0$  and  $P_0$ . For example, in section 3 I will use the numerical simulator TOUGH2 [Pruess et al., 1999] to calculate the amplitude changes.

[38] One can gain some physical insight into the meaning of the phase terms  $\theta_s$  and  $\theta_p$  following a line of reasoning first suggested by Virieux et al. [1994]. I discuss this approach in some detail in Appendix C. Note that each of the semianalytic expressions (51) and (52) contain temporal integrals of an exponential of the phase function multiplied by an amplitude function. The exponential of the phase function is always a positive number, and the amplitude function is typically of one sign for a passing front. For example, the amplitude function  $S_0$  will either describe a decrease or an increase in the saturation of the aqueous phase, depending on the nature of the passing coupled front. Thus, the integrals are typically piecewise monotonic if the coupled multiphase front is a result of the injection of a particular fluid component.

[39] As noted by Vasco et al. [2000] and Vasco and Fisterle [2004], for a step function source, the transient, wave-like nature of a solution to the diffusion equation is emphasized by taking the derivative of the head or pressure with respect to time. Thus, I shall be interested in the time derivatives of the saturation and pressure changes, which are of the form

$$\frac{\partial \bar{S}(\mathbf{X}, T, \theta_s)}{\partial t} = e^{\theta_s(\mathbf{X}, T)} S_0(\mathbf{X}, T) \quad (53)$$

$$\frac{\partial \bar{P}(\mathbf{X}, T, \theta_p)}{\partial t} = e^{\theta_p(\mathbf{X}, T)} P_0(\mathbf{X}, T). \quad (54)$$

[40] For a separable phase function, as given by equation (50), the saturation and pressure resemble the product of a

Gaussian function and the time-varying amplitude function. In Appendix C I derive a relationship between the phase function  $\theta$  and the arrival time of the pressure and saturation fronts  $T_{\text{peak}}$  for a separable phase function with a power law time dependence:

$$\sqrt{T_{\text{peak}}} = \frac{1}{2\sqrt{\alpha_s}} \int_{x(s)} \sqrt{\Omega} ds, \quad (55)$$

where  $\Omega$  is given by expression (40).

### 3. Applications

[41] In this section I illustrate how one can use the expression for the slowness, equation (41), to calculate the travel time of a coupled pressure and saturation disturbance. For simplicity, I shall neglect gravitational effects, so that equation (41) reduces to

$$p^2 - \Omega \frac{\partial \theta}{\partial t} = 0. \quad (56)$$

[42] In the examples that follow I shall consider the injection of water into a layer containing a nonaqueous phase liquid (NAPL). For the first two illustrations the layer is homogeneous, the permeability is  $2 \times 10^{-13}$  m/s, and the porosity is 0.10. For simplicity, there are no capillary effects in these examples. In the last illustration the layer is heterogeneous.

[43] The numerical simulator TOUGH2 [Pruess *et al.*, 1999] is used to model the flow of the two phases in response to the injection. The relative permeability functions  $k_{rw}(S)$  and  $k_{rn}(S)$  are plotted in Figure 1. The relative permeability of the nonaqueous phase liquid is given by the default formulation of TOUGH2 [Pruess *et al.*, 1999, p. 50] for oil,

$$k_{rn}(S) = \frac{1 - S - S_{nr}}{1 - S_{nr}}, \quad (57)$$

where  $S_{nr}$  is the residual saturation of the NAPL. The relative permeability function described by Corey [1954] is used to model the water,

$$k_{rw}(S) = \hat{S}^4, \quad (58)$$

where

$$\hat{S} = \frac{S - S_{wr}}{1 - S_{wr} - S_{gr}} \quad (59)$$

and  $S_{wr} = 0.2$ ,  $S_{nr} = 0.01$ , and  $S_{gr} = 0.1$ . Other relative permeability functions [Fatt and Klikoff, 1959; Brooks and Corey, 1966; Mualem, 1976; van Genuchten, 1980] are certainly possible, and their substitution would involve no extra work.

[44] A central well, indicated by a star in Figure 2, injects water at a rate of 4.0 kg/s. The injection starts at time zero and continues at a constant rate. Thus, the source behaves as a step function in time. Two observation points, located to the north of the injector, are denoted by the open

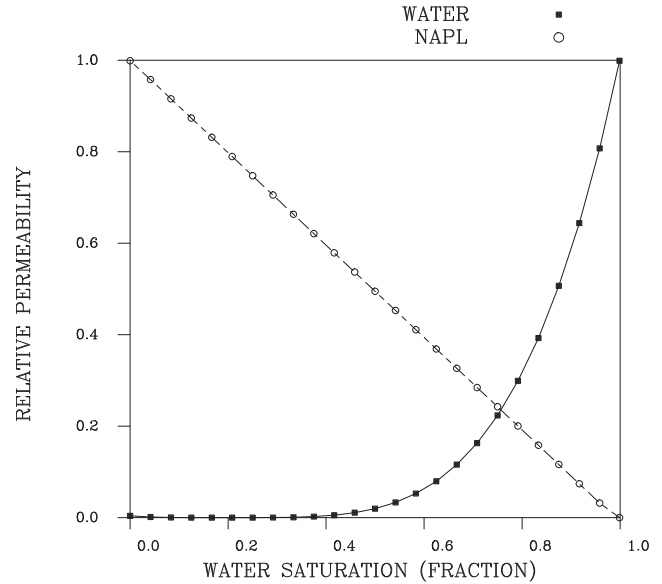


**Figure 1.** Relative permeability curves for the nonaqueous phase liquid (NAPL) and for water as a function of the water saturation. The nonaqueous phase liquid function is the default for oil in the reservoir simulator TOUGH2 [Pruess *et al.*, 1999].

and filled circles in Figure 2. Because of the injection, saturation and pressure changes propagate from the injection well into the porous layer. The water saturation and pressure distributions, after 100 days of injection, are shown in Figure 2.

[45] The saturation changes and the pressure calculated at the first observation point, denoted by the filled circle in Figure 2, are shown in Figure 3. Note that saturation and pressure changes occur soon after the start of injection. Initially, there is a small decrease in water saturation at the observation point. However, a large, rapid saturation increase occurs around 250 days after the start of injection. In contrast, the pressure builds up gradually and monotonically over time. Careful examination of the pressure variation in Figure 3 indicates a change in the rate of pressure buildup at around 250 days. As noted here and in previous publications [Vasco *et al.*, 2000; Vasco and Finsterle, 2004; Vasco, 2008a], the propagation of transient pressure changes is clearer if one considers the time derivative of the pressure history. To this end, I plot the time derivative of both the saturation and pressure changes in Figure 4. Note that the time derivative of the pressure displays two peaks, the first at an early time (less than 100 days) and the second around 300 days. The derivative of the saturation change, shown in Figure 4a, displays similar characteristics, in this case a trough at an early time and a peak at around 300 days. In section 3.1 I shall examine the early changes, which I refer to as the first arrival, in more detail. Because the change in saturation associated with the early disturbance is quite small, less than 5%, the flow in this case is dominated by the larger change in pressure.

#### 3.1. Flow Dominated by a Change in Pressure

[46] The changes at early times are associated with the transient pressure disturbance propagating in the nonaqueous

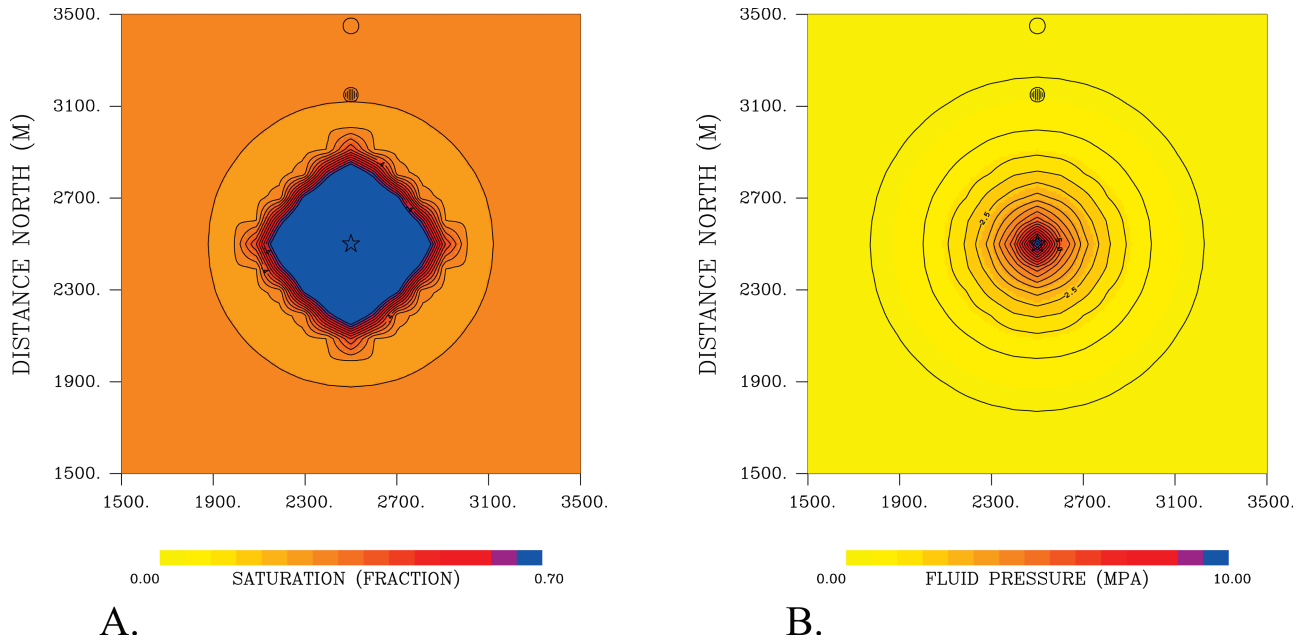


**Figure 2.** (a) The distribution of water saturation in the porous layer after 100 days of water injection. The two observation points are denoted by the filled and open circles. (b) The pressure field after 100 days of injection.

phase liquid, well ahead of the injected water front. That is, the saturation and pressure changes are dominated by pressure propagation through the background saturation distribution. There is also a small saturation change driven by the pressure changes, inducing relative flow of the two phases. In this section I shall consider these changes and interpret them in terms of the expressions for the travel time and phase velocity.

[47] The early peak in the pressure derivative in Figure 4 is shown in greater detail in Figure 5. In Figure 5 I have also plotted the early decrease in saturation seen in Figure

4a. Both of these curves have been normalized to unit amplitude and converted so that they are both positive. Note how closely the pressure change follows the saturation change in time (Figure 5), with a peak value at around 50 days. One can also consider snapshots of the normalized saturation and pressure derivatives in the layer. Specifically, I plot the normalized saturation and pressure derivatives in each grid block at particular times in Figures 6 and 7. These snapshots convey the transient propagation of the saturation and pressure changes. That is, the peak of the saturation and pressure derivatives propagates outward from the

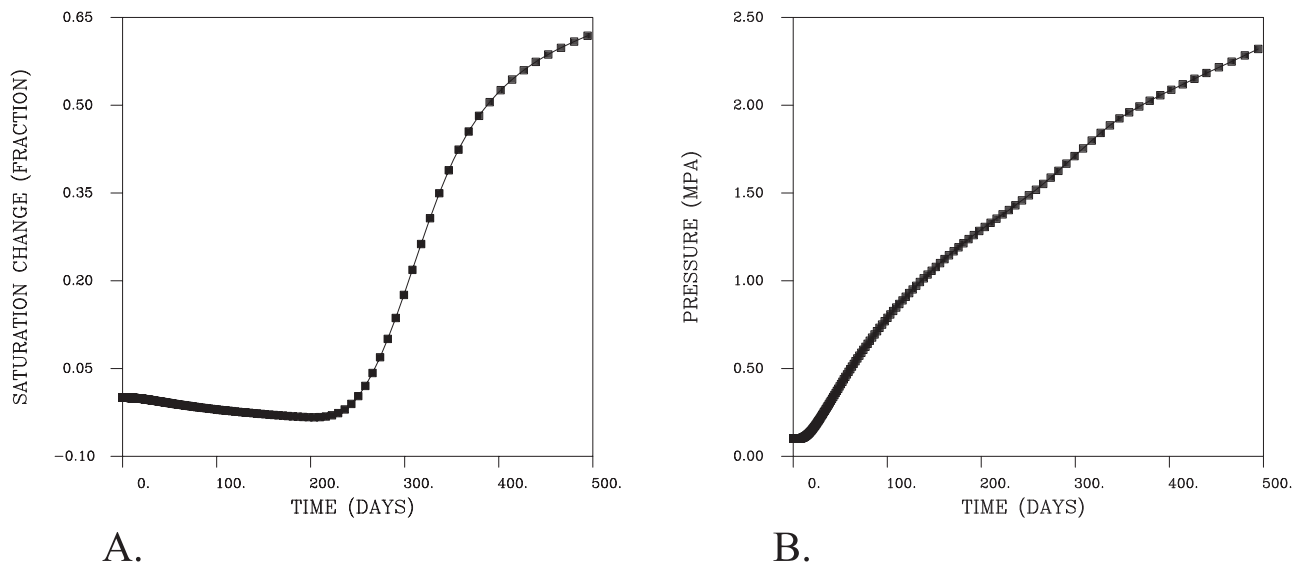


**Figure 3.** (a) Time-varying saturation change at the first observation point (indicated by the filled circle in Figure 2). (b) Time-varying pressure at the first observation point.

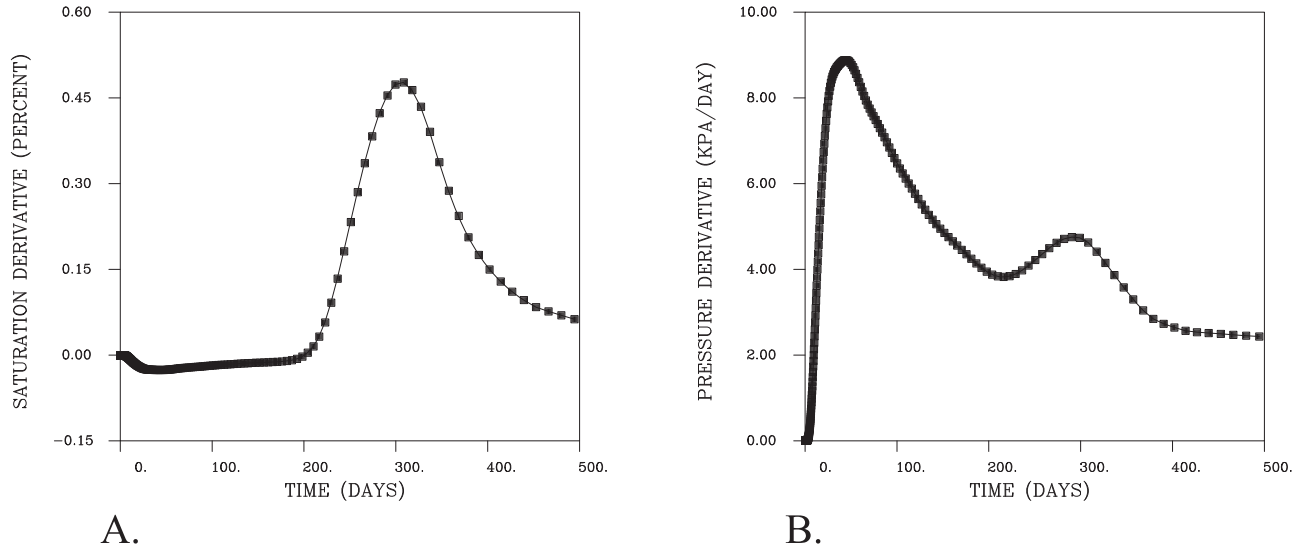


**Figure 4.** (a) Time derivative of the saturation change. (b) Time derivative of the pressure variation at the first observation point.

injection well over time. Furthermore, the changes in saturation and pressure are coupled and move with the same velocity. That is to be expected because the saturation changes are induced by the propagating pressure changes. Noting the time at which the normalized derivative of the saturation and pressure in each grid block attains a maximum value, I can compute the arrival time of the disturbances at each point in the layer (Figure 8). The arrival times are very similar for the early-time saturation and pressure changes.

[48] Using the expressions for  $\Omega$ , equation (40), and the travel times (equation (55)), one can estimate the arrival times for the saturation and pressure changes. When there

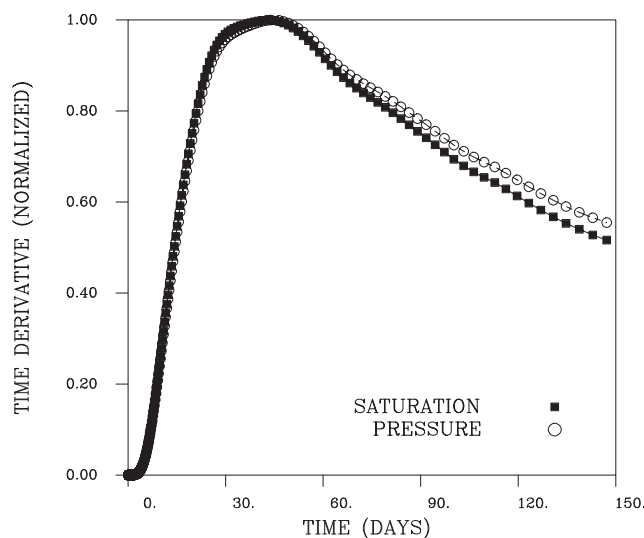


**Figure 5.** Normalized time derivatives of the saturation and pressure variations for the first 150 days from the start of water injection. The derivatives are normalized such that the peak values are 1.

is only a small saturation change associated with the propagating front, I can approximate the coefficient  $\Omega$  by

$$\Omega = \frac{\alpha_T [(1 - S_b) \eta_n^{-1} - \chi S_b \eta_w^{-1}]}{k(1 - \chi)}, \quad (60)$$

where  $\alpha_T$  is the proportionality coefficient in equation (10), a function of the compressibilities of the poroelastic system. Note that (60) only depends upon the properties of the medium. As noted by *Vasco and Finsterle* [2004], one can use the arrival time field estimated from the output of the numerical simulator to compute the trajectories  $\mathbf{x}(t)$  defined by equations (46) and (47). In Figure 8 I have plotted the trajectory from the second observation point, denoted by the open circle, to the injection well, denoted by the star. Because the layer is homogeneous the trajectory is a straight line. Using expressions (55) and (60), I can estimate the travel time, assuming that the pressure disturbance travels in the same manner as a solution to the diffusion equation:

$$\sqrt{T_p} = \frac{1}{6} \int_{\mathbf{x}} \sqrt{\frac{\alpha_T [(1 - S_b) \eta_n^{-1} - \chi S_b \eta_w^{-1}]}{k(1 - \chi)}} d\mathbf{s}. \quad (61)$$

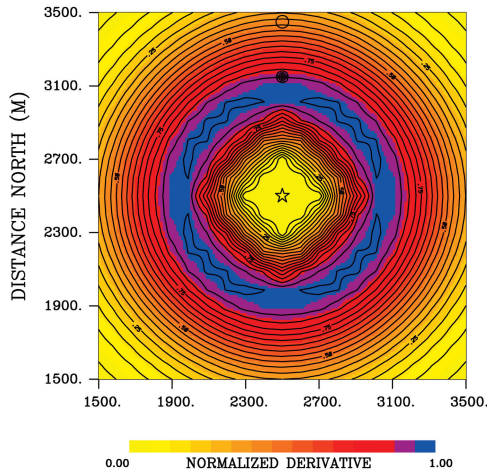
[49] In Figure 9 I compare travel times estimated using equation (61) to estimates extracted from the output of the TOUGH2 numerical simulation. The values are computed for the points along the trajectory shown in Figure 8. In general, there is good agreement between the semianalytic estimates based upon equation (61) and the estimates from the numerical simulator.

### 3.2. Fully Coupled Saturation and Pressure Changes

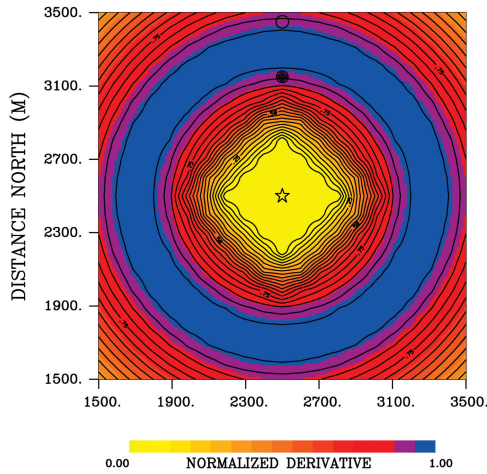
[50] Now consider the second arrival in Figure 4, associated with the propagating saturation front. One can no longer assume that the saturation change is small. Neither can one assume that the pressure change is negligible because

# Saturation

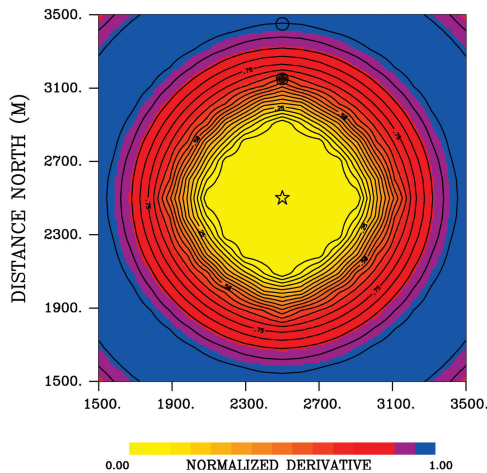
## 30 Days



## 60 Days



## 120 Days



of its large magnitude. To some degree I can isolate the pressure change by calculating the pressure field in the layer because of the injection of fluid of the same composition. Thus, I can estimate the component of the pressure change due to the fluid mass change with no corresponding saturation change. In Figure 10 I compare the derivative of this differential pressure, normalized such that the peak of the time derivative is unity, to the normalized time derivative of the saturation change. The removal of the pressure change because of the fluid mass change is imperfect; however, in general, there is good agreement between saturation and pressure. As for the earlier phase, I can examine snapshots of the saturation and pressure time derivatives as they vary over the simulation grid (Figures 11 and 12). Again, the propagation of the disturbance is apparent in the snapshots, as is the agreement between the saturation and pressure changes. Note that the propagation away from the injection point is not entirely symmetric, indicating some anisotropy, likely because of numerical grid effects. This effect could possibly be minimized by taking a finer simulation grid. In order to minimize the grid effects I consider observation points along the north-south axis of the grid, denoted by the filled and open circles in Figures 11, 12, and 13.

[51] As was done for the first arrival, one can postprocess the results of the numerical simulation in order to estimate travel times for the propagating disturbances. The simplest approach, and the one taken here, is to take the time at which the time derivative attains a maximum value as the arrival time of the disturbance. In Figures 13a and 13b I have plotted the travel times associated with the saturation and pressure disturbances, respectively. There is excellent agreement between the two distributions of travel times within the layer. Note that the anisotropy, possible because of numerical grid effects, is reflected in the asymmetry of the travel time contours. The trajectories, computed by marching down gradient of the travel time functions, are also shown in Figure 13. The trajectories denote the path traveled by the saturation and pressure disturbances from the injection well to the outer observation point, denoted by the open circle.

[52] Using the expression for  $\Omega$ , given by equation (40), one can calculate the travel time from the medium parameters and the changes in saturation and pressure because of the passage of the two-phase front. The model for water and NAPL in TOUGH2 assumes no capillary effects so that the functions  $\gamma_c$  and  $\Upsilon$  vanish and  $\Omega$  takes the form

$$\Omega = \frac{\alpha_T [(1 - S_b) \eta_n^{-1} - \chi S_b \eta_w^{-1}]}{k(1 - \chi)} + \frac{\varphi [\chi \eta_w^{-1} + \eta_n^{-1}] \bar{S}}{k(1 - \chi) \bar{P}}. \quad (62)$$

[53] From (62) and the relationship between  $\Omega$  and  $T_{\text{peak}}$ , as given in equation (55), it is clear that the second term is responsible for the additional time taken to travel from the injection well to the observation point. The amplitude changes  $\bar{S}$  and  $\bar{P}$  were estimated from the numerical simulator output. Specifically, I compute the difference between

**Figure 6.** Snapshots of the normalized time derivative of the saturation variation for three different times. The time derivative of the saturation variation in each grid block is formed and normalized such that its peak value is 1.

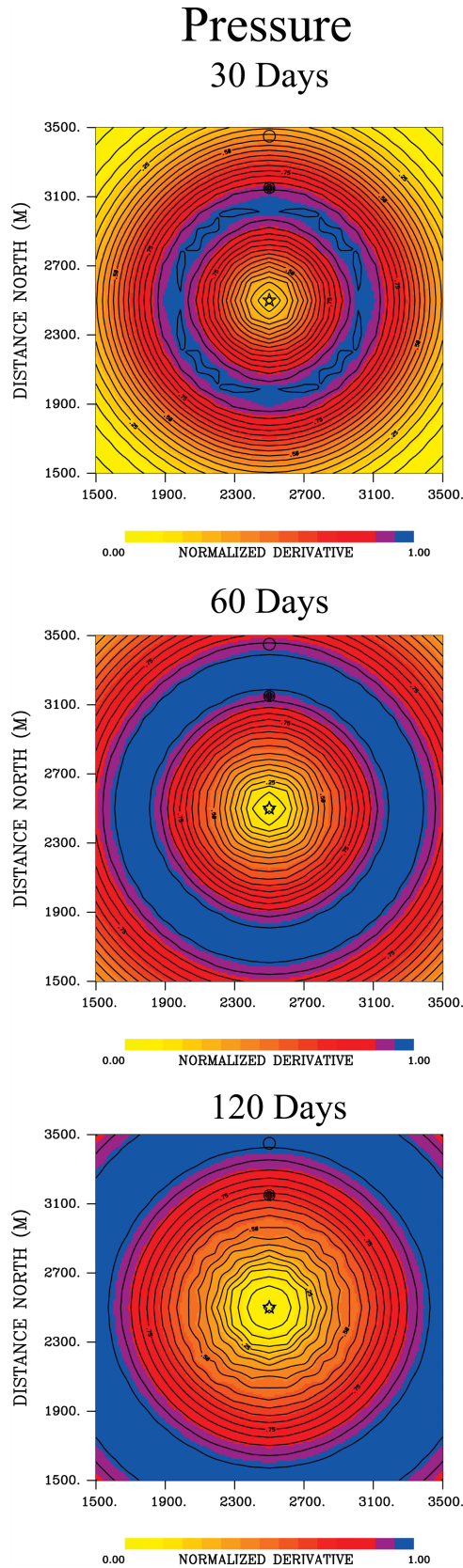


**Figure 7.** Snapshots of the normalized time derivatives of the pressure variation for three different times. The time derivative of the pressure variation in each grid block is formed and normalized such that its peak value is 1.

the field values associated with the arrival time of the front (the time at which the time derivative is a maximum) and the field values before the arrival of the front. Note that the saturation changes because of the passage of the two-phase front are primarily controlled by the background saturation and the relative permeability characteristics of the reservoir, for example, by the irreducible water saturation. In Figure 14 I compare the travel time estimates based upon (62) with the times obtained by postprocessing the TOUGH2 numerical simulator saturation and pressure histories. In general, there is good agreement between the saturation and pressure arrival times computed from the TOUGH2 simulation and the asymptotic estimates.

### 3.3. Flow in a Heterogeneous Medium

[54] As noted, one motivation for developing semianalytic solutions is the solution of the inverse problem. That is, one would like to use the explicit expressions to develop efficient and flexible methods for characterization. For this reason, I have allowed for heterogeneity of arbitrary magnitude in the formulation. In this subsection I consider a heterogeneous medium, described by a variation in absolute permeability  $k(\mathbf{x})$ ; all other parameters are kept at the values used in the homogeneous case. The smoothly varying model contains generally higher permeability to the west and lower permeability to the east (Figure 15). The lowest permeability is found in the northeast corner of the model. The saturation and pressure variations, in response to water injection in the central well, are influenced by the heterogeneity. This is clear in Figure 16, which displays the saturation and pressure variations in the layer after 525 days of injection. The fields reflect the heterogeneity, with rapid migration of the two-phase front in the higher-permeability region west of the injection well.

[55] The saturation and pressure histories are calculated at an observation point to the north of the injector, indicated by the filled circle in Figure 16. In Figure 17 the time derivatives of the saturation and pressure variations are plotted as a function of time from the start of injection. The overall character of the curves, the two peaks in the pressure derivative and the early decrease in saturation followed by a large and rapid increase, are similar to those found in the homogeneous case (Figure 4). As in the homogeneous case, I can compute the travel times associated with the two sets of extrema in the saturation and pressure variations. For example, the first arrival time is associated with the first peak in the pressure derivative, as seen in Figure 17b, and the early trough in the saturation variation (Figure 17a). The distributions of travel times for the saturation and pressure variations are shown in Figures 18a and 18b, respectively. The distributions of travel times are very similar, as are the trajectories computed by marching down the gradient of the travel time field from an observation point to the injection point (Figure 18). Using equation (61), now with a spatially varying absolute permeability  $k(\mathbf{x})$ , I can calculate the travel time for the heterogeneous medium. In Figure 19 I compare the estimated travel times to values obtained from the numerical simulation. The travel times are computed for points along the trajectory shown in Figure 18. The asymptotic estimates are in general agreement with travel times obtained from the TOUGH2 simulator output. In general, the front moves

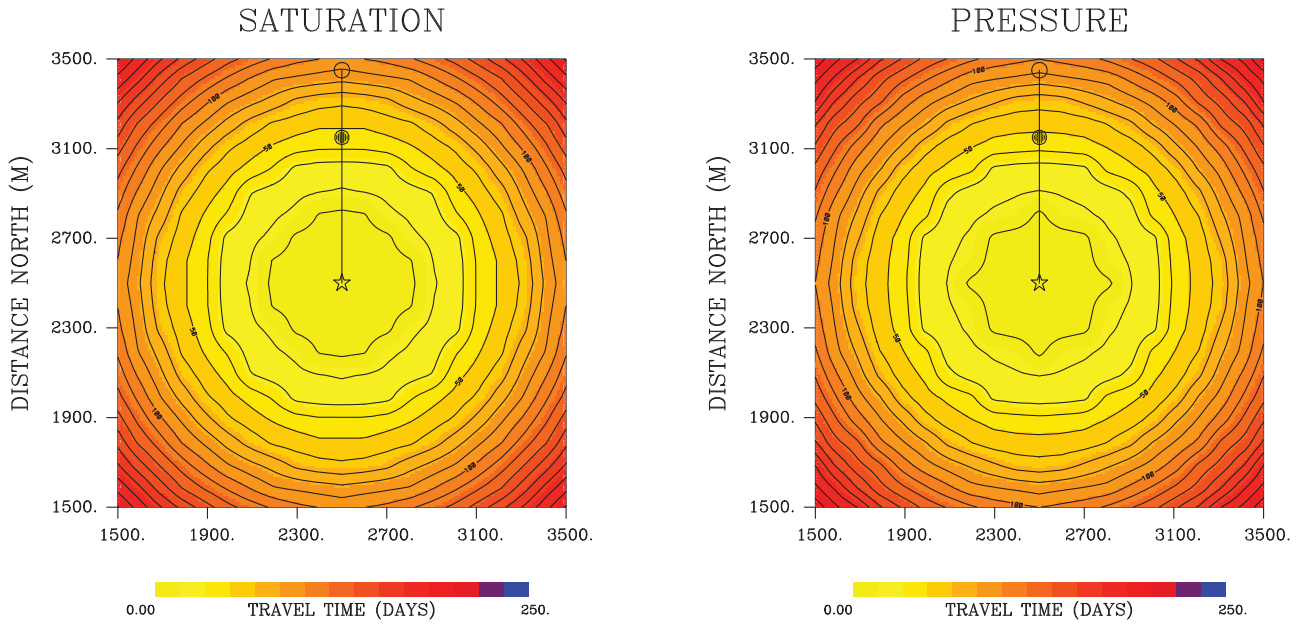


**Figure 8.** Contour plots of the phase function computed from the saturation and pressure variations in each block of the simulation grid. The two observation points are signified by the filled and unfilled circles. Trajectories, extending from the second observation point to the injection well, are denoted by the solid lines.

faster at near and intermediate distances and then slows considerably at farther offsets. This behavior makes physical sense because as seen in Figure 15, the trajectory encounters lower permeability material as it traverses the northeast quadrant of the simulation grid near the end of the path.

[56] Now I consider the later arrival, exemplified by the second peak in the saturation and pressure derivatives in Figure 17. As noted, this disturbance is due to the propagating saturation front, and the travel time is related to the variable  $\Omega$ , given by (62). In this case, the absolute permeability  $k(\mathbf{x})$  is a spatially varying quantity. I should point

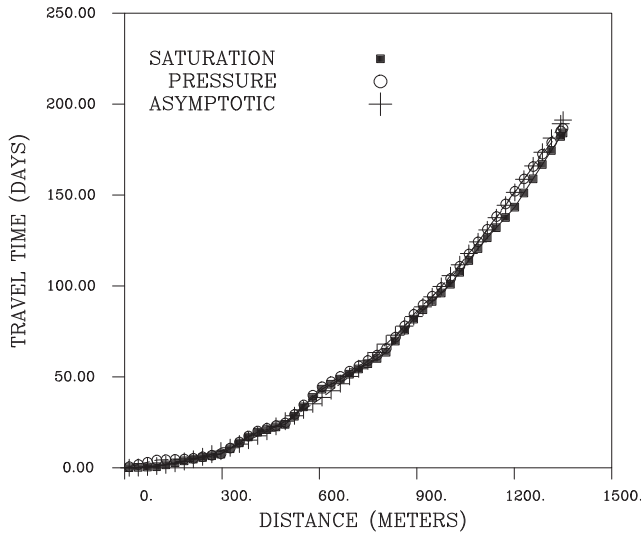


**Figure 9.** Travel times associated with various points along the trajectories shown in Figure 8, which extend from the second observation point to the injection well. The travel times for the saturation and pressure phase functions are associated with the time at which the derivative attains its maximum value. The travel times calculated using the asymptotic expression (see equation (61)) are also plotted for points along the trajectory.

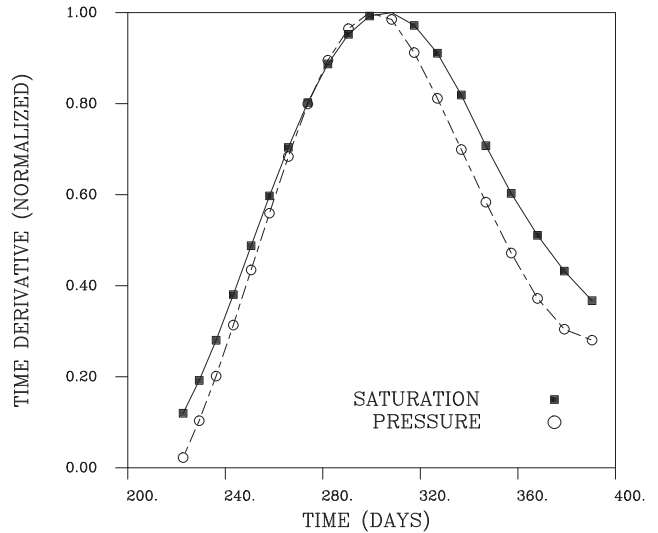


**Figure 10.** Time derivatives of the saturation and pressure variations at the first observation point (denoted by a filled circle in Figure 1). The derivatives have been normalized such that the peak values are 1. The values are associated with the second set of peaks, between 200 and 400 s, in Figure 4. A background pressure variation, calculated for oil injection in an oil-saturated layer, has been removed from the pressure curve.

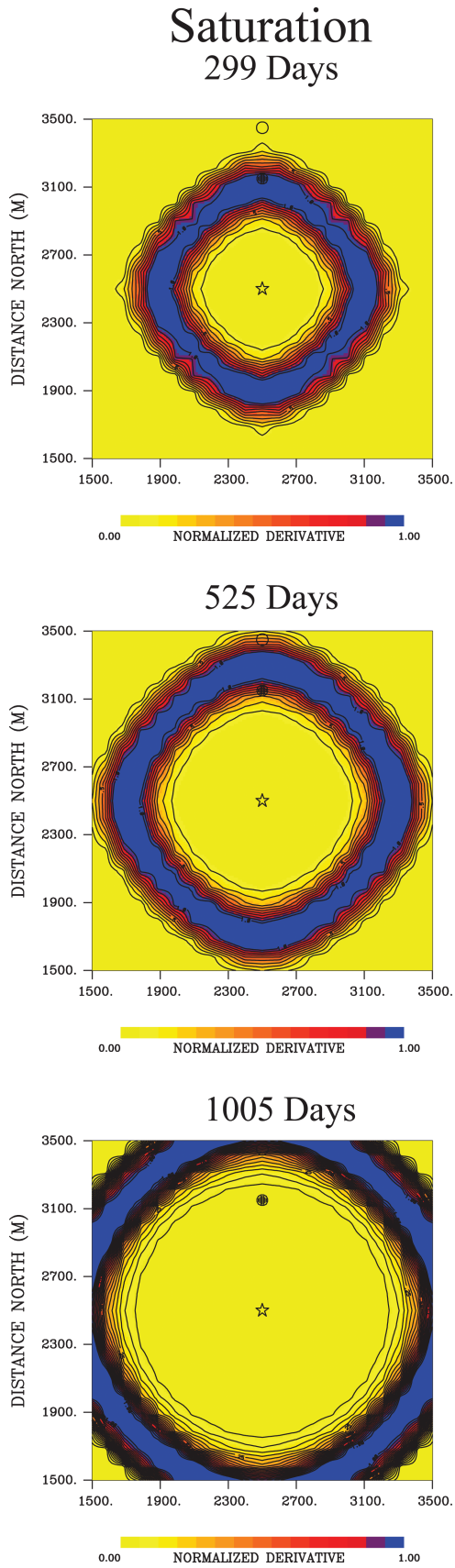


Figure 11. Snapshots of the normalized time derivatives of the saturation variation in each grid block.

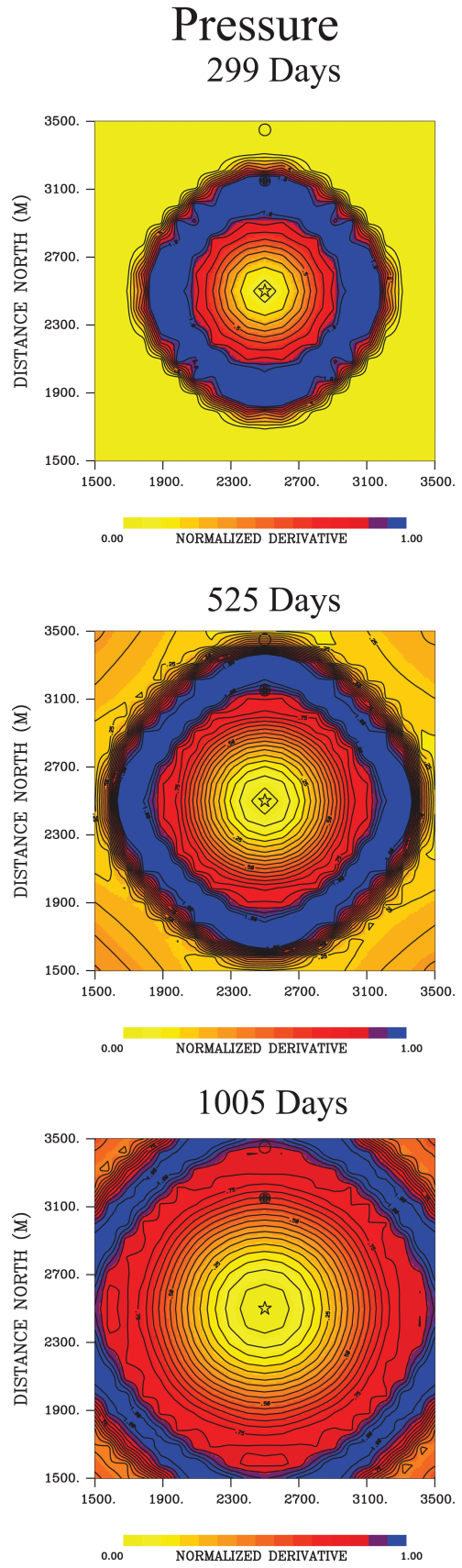
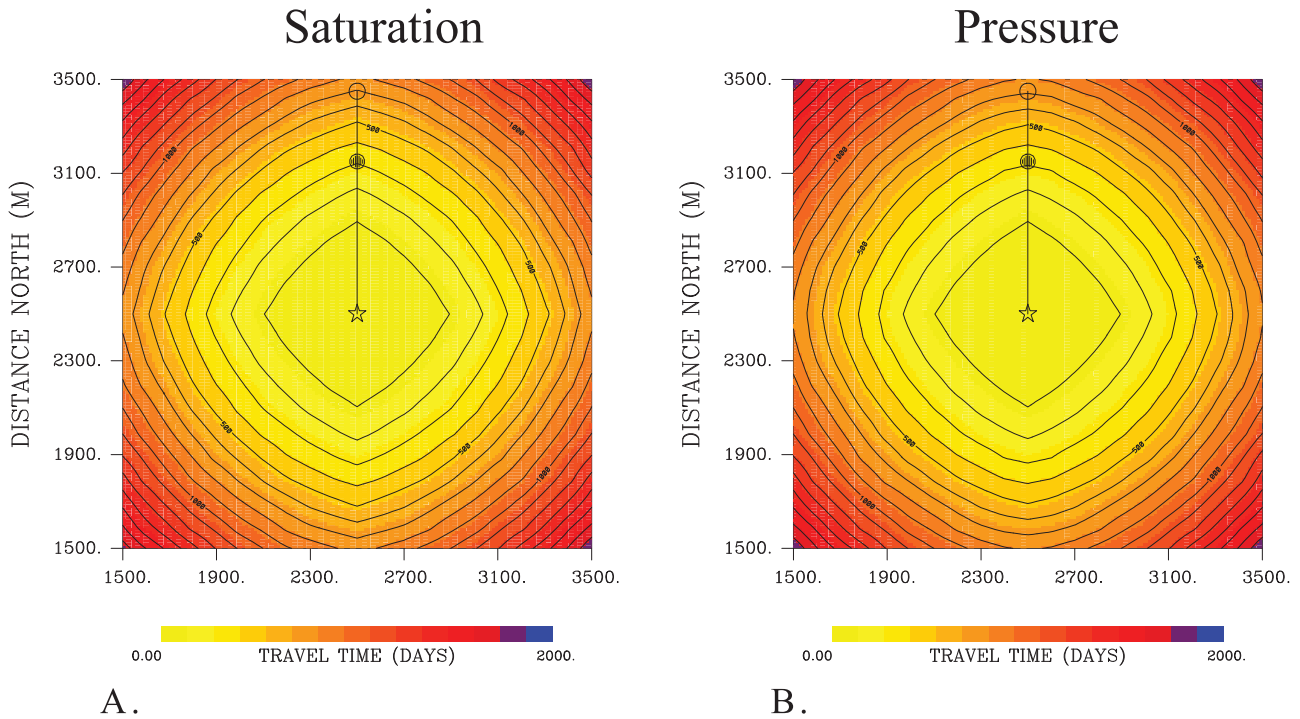


Figure 12



**Figure 13.** Contour plots of the phase function computed from the saturation and pressure variations in each block of the simulation grid. The phase functions correspond to the second set of peaks in Figure 4, the second arrival. The two observation points are signified by the filled and unfilled circles. Trajectories, extending from the second observation point to the injection well, are denoted by the solid lines.

out that the permeability appears both explicitly in (62) as well as implicitly, as the permeability also determines the saturation and pressure amplitude changes,  $\bar{S}$  and  $\bar{P}$ , respectively. Thus, the travel time distribution and the trajectories for this disturbance can differ from those of the first arrival. In fact, the travel time contours and the trajectory for the second arrival (Figure 20) do differ from those of the first arrival (Figure 18). Some of the differences may also be because of grid orientation effects, noted in Figures 11, 12, and 13. In both cases the trajectories curve toward the higher-permeability region, away from areas of lower permeability. Using (62), I calculate the expected travel time to points along the trajectory, as shown in Figure 21. As in the homogeneous case, the travel time is much greater for the second arrival because of the presence of the second term in equation (62). Also, as for the first arrival, the disturbance travels faster to near and intermediate points of the trajectory and takes much longer to reach the more distant points.

#### 4. Conclusions

[57] Under the assumption of smoothly varying heterogeneity, it is possible to derive an explicit equation for the phase velocity of a coupled change in saturation and fluid pressure. The expression displays the dependence of the front velocity upon the parameters of the medium and the saturation and pressure changes that occur as the front

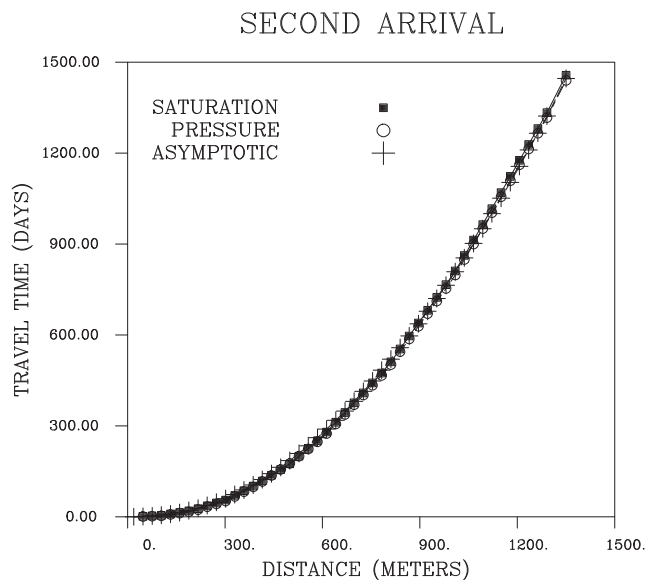


**Figure 14.** Travel time to points at various distances along the trajectories plotted in Figure 13. The saturation and pressure estimates were obtained by postprocessing the output of the numerical simulator TOUGH2 [Pruess et al., 1999]. The asymptotic estimates, based upon the expression (62), are denoted by the crosses.

**Figure 12.** Snapshots of the normalized time derivatives of the pressure variation in each grid block. A background pressure variation, calculated for oil injection in an oil saturated layer, has been removed from the pressure curve in each grid block.

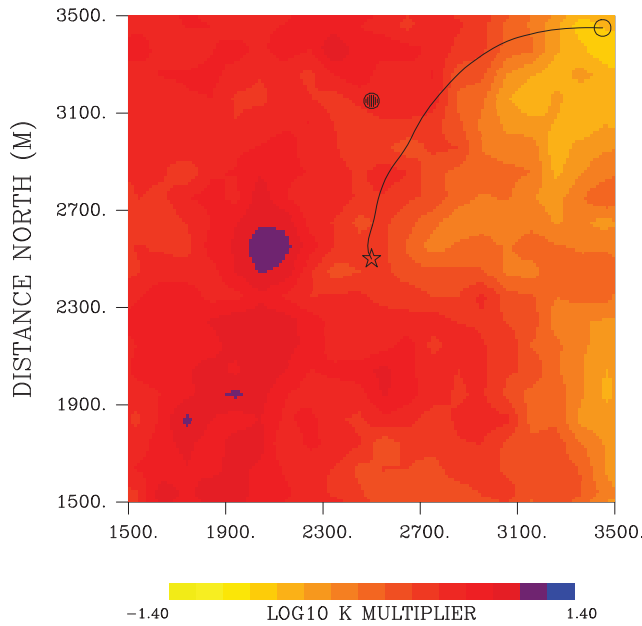


**Figure 15.** Permeability model used in the heterogeneous test case. Darker colors denote higher permeability. Two observation points are indicated by the filled and unfilled circles. The injection well is denoted by the star, and the trajectory is a curve connecting the outermost observation point with the injection well.

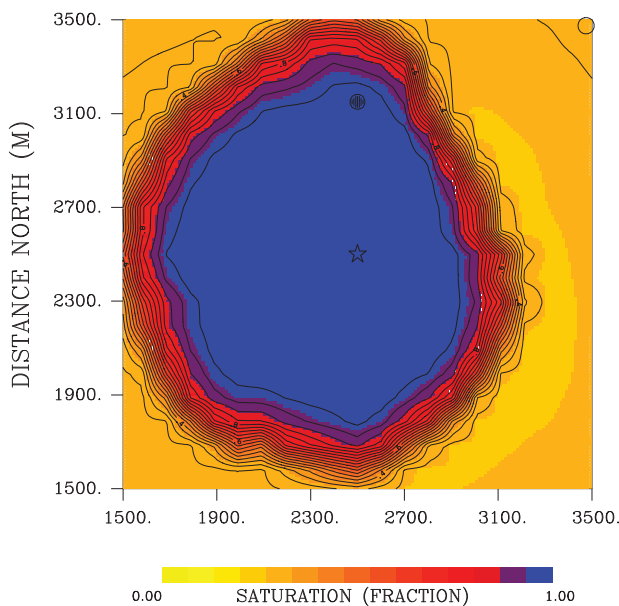
passes. Because of the presence of the saturation and pressure amplitude changes, the expression for the front velocity is evaluated in conjunction with a numerical simulation.

[58] The presence of the saturation and pressure amplitudes means that at least two modes of propagation are pos-

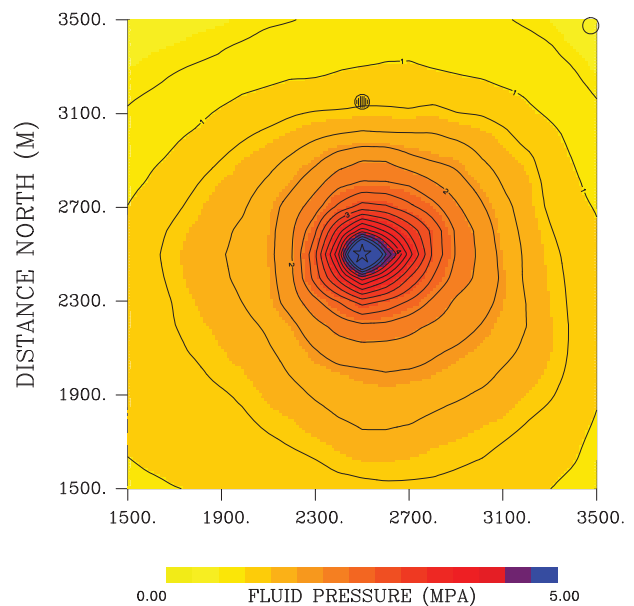
sible, depending on the relative magnitude of the saturation and pressure changes. That is, the coupled front can propagate with a different velocity depending on the size of the saturation change relative to the change in pressure as the front passes. Numerical simulation using TOUGH2 [Pruess *et al.*, 1999] indicates that two modes of propagation are important: the propagation of a pressure-dominated change and the propagation of a coupled front in which the saturation change is also large. These conclusions hold for a heterogeneous medium, though the geometry is controlled by the spatial variation of properties. The factors influencing the propagation velocity of the two-phase front are the background saturation, the saturation-dependent components of the fluid mobilities, the medium compressibility, the permeability, the porosity, and the ratio of the slopes of the relative permeability curves at the background saturation.

[59] Note that while it is indeed possible to observe the two coupled arrivals in the results of the numerical simulation, as in Figure 4, the asymptotic analysis provides a quantitative interpretation in terms of the medium parameters and the pressure and saturation changes (see equation (40) and the reduced forms (60) and (62)). Furthermore, while the arrivals are clear in the pressure and saturation derivatives plotted in Figure 4, their expression in the actual pressure and saturation variations (Figure 3) are rather subtle. It might be difficult to detect the saturation and pressure variations induced by the two propagating disturbances without the guidance provided by the asymptotic analysis.

[60] The asymptotic methodology results in solutions that are defined along trajectories, similar to ray methods in high-frequency electromagnetic [Kline and Kay, 1965] and elastic wave propagation [Karal and Keller, 1959].



A.



B.

**Figure 16.** (a) Distribution of water saturation in the heterogeneous porous layer after 525 days of water injection. The two observation points are denoted by the filled and open circles. (b) The pressure field after 525 days of injection.

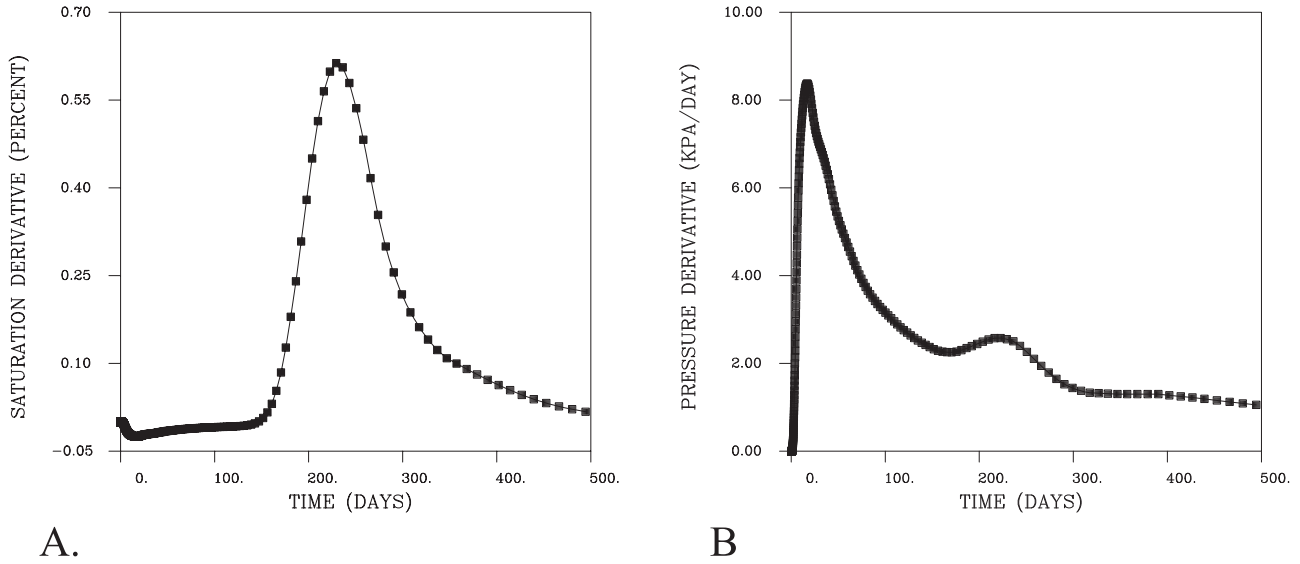


**Figure 17.** (a) Time derivative of the saturation change. (b) Time derivative of the pressure variation at the first observation point.

Streamline simulation is another technique for modeling multiphase flow that leads to solutions defined along trajectories [Datta-Gupta and King, 1995]. There are differences between the approach taken here and streamline simulation. Streamline approaches usually account for gravity using an additional step, such as operator splitting. In this paper gravity is incorporated directly. Streamline methods do not account for capillary effects when computing the trajectory

ries. In the approach taken in this paper, capillary effects are contained in the function  $\Omega$  through the variables  $\Upsilon$  and  $\gamma_c$  and influence the phase function and, hence, the trajectories.

[61] The techniques described here are general and may be applied to any system of nonlinear partial differential equations. Thus, one may consider coupled processes involving deformation and thermal effects [Vasco, 2010].

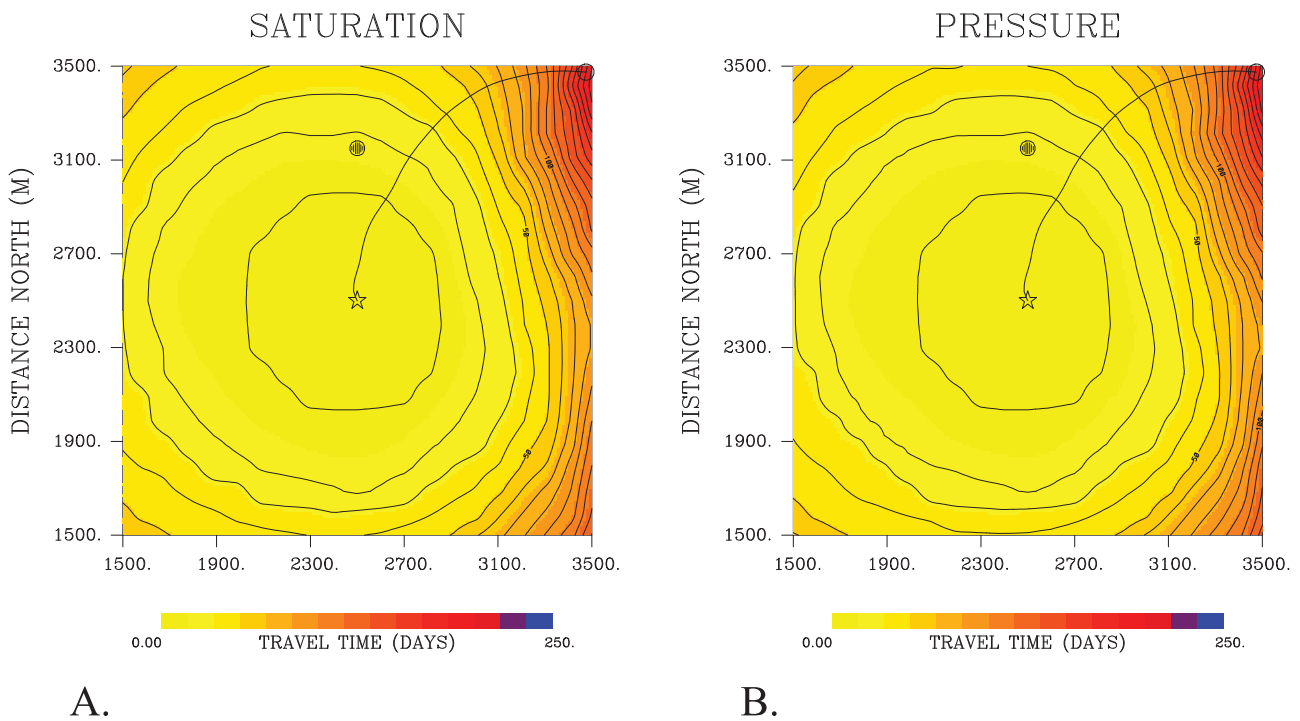


**Figure 18.** Contour plots of the phase function computed from the (a) saturation and (b) pressure variations in each block of the simulation grid. The two observation points are signified by the filled and unfilled circles. Trajectories, extending from the second observation point to the injection well, are denoted by the solid lines.

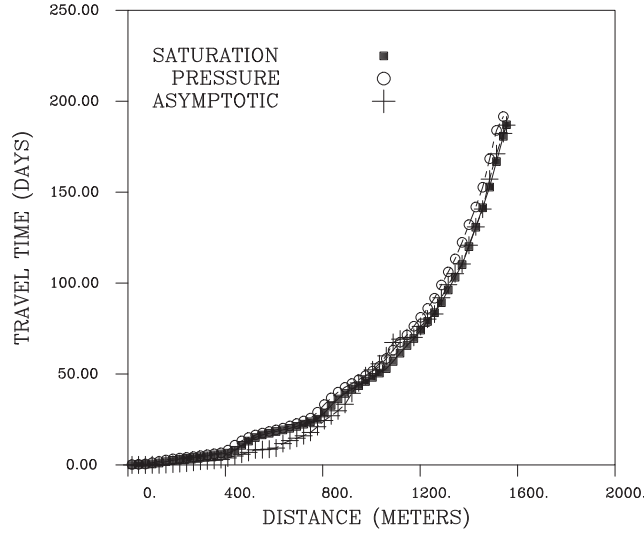


**Figure 19.** Travel times associated with various points along the trajectories shown in Figure 18, which extend from the second observation point to the injection well. The travel times for the saturation and pressure phase functions are associated with the time at which the derivative attains its maximum value. The travel times calculated using the asymptotic expression (see equation (61)) are also plotted for points along the trajectory.

However, as additional variables and equations are added, the resulting expressions for the phase velocity become increasingly complicated. The increased complexity is no different from that seen in linear systems, such as in

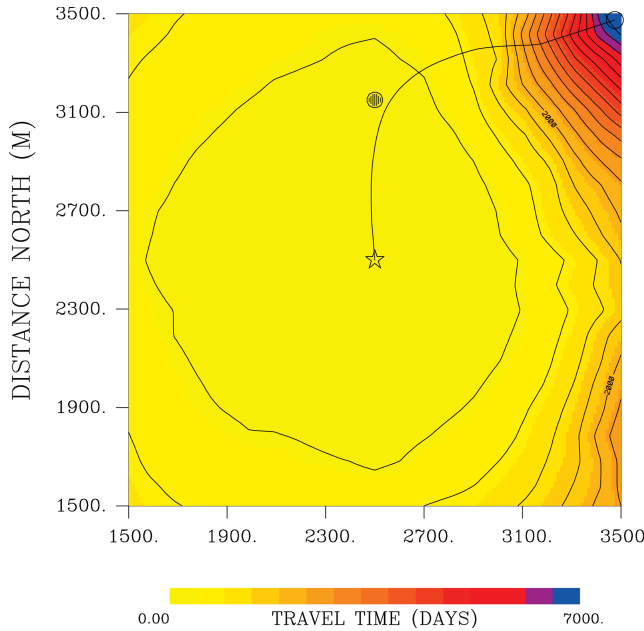


**Figure 20.** Contour plots of the phase function computed from the saturation variations in each block of the simulation grid. The phase function corresponds to the second peak in Figure 17, the second arrival. The two observation points are signified by the filled and unfilled circles. A trajectory, extending from the second observation point to the injection well, is denoted by the solid line.

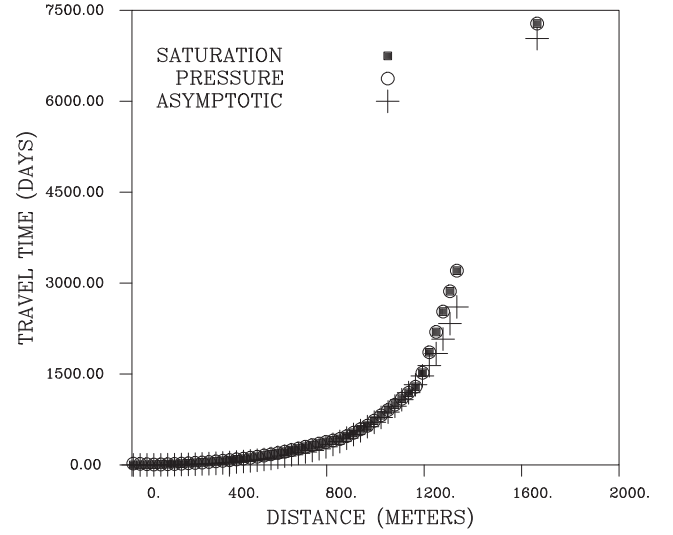


**Figure 21.** Travel times associated with various points along the trajectory shown in Figure 20, which extends from the second observation point to the injection well. The travel times for the saturation phase function are associated with the time at which the derivative attains its maximum value. The travel times calculated using the asymptotic slowness expression (see equation (62)) are also plotted for points along the trajectory.

coupled deformation in a poroelastic medium saturated with two fluid phases [*Tuncay and Corapcioglu, 1996*].

## Appendix A: Method of Multiple Scales

### A1. First of the Governing Equations

[62] Consider the first of the governing equations (14) and its representation in terms of the slow coordinates  $\mathbf{X}$  and  $T$ . Substituting for the differential operators in this equation gives the expression

$$\begin{aligned}
 & \varepsilon \nabla \kappa \cdot \left( \varepsilon \nabla P + \nabla \theta_p \frac{\partial P}{\partial \theta_p} \right) \\
 & + \chi_w \left( \varepsilon \nabla S + \nabla \theta_s \frac{\partial S}{\partial \theta_s} \right) \cdot \left( \varepsilon \nabla P + \nabla \theta_p \frac{\partial P}{\partial \theta_p} \right) \\
 & + \varepsilon \nabla \cdot \left( \varepsilon \nabla P + \nabla \theta_p \frac{\partial P}{\partial \theta_p} \right) \\
 & + \nabla \theta_p \frac{\partial}{\partial \theta_p} \left( \varepsilon \nabla P + \nabla \theta_p \frac{\partial P}{\partial \theta_p} \right) \\
 & - \rho_w \varepsilon \nabla k \cdot \mathbf{Z} \\
 & - \rho_w \chi_w \left( \varepsilon \nabla S + \nabla \theta_s \frac{\partial S}{\partial \theta_s} \right) \cdot \mathbf{Z} \\
 & = \frac{\alpha_T}{k \eta_w} S \left( \varepsilon \frac{\partial P}{\partial T} + \frac{\partial \theta_p}{\partial t} \frac{\partial P}{\partial \theta_p} \right) \\
 & + \frac{\phi}{k \eta_w} \left( \varepsilon \frac{\partial S}{\partial T} + \frac{\partial \theta_s}{\partial t} \frac{\partial S}{\partial \theta_s} \right).
 \end{aligned} \tag{A1}$$

[63] Expanding the product terms and retaining terms of order  $\varepsilon^0 \sim 1$  gives

$$\begin{aligned} & \chi_w \nabla \theta_s \cdot \nabla \theta_p \frac{\partial S}{\partial \theta_s} \frac{\partial P}{\partial \theta_p} + \nabla \theta_p \cdot \nabla \theta_p \frac{\partial^2 P}{\partial \theta_p^2} - \rho_w \chi_w \nabla \theta_s \cdot \mathbf{Z} \frac{\partial S}{\partial \theta_s} \\ &= \frac{\alpha_T}{k\eta_w} S \frac{\partial \theta_p}{\partial t} \frac{\partial P}{\partial \theta_p} + \frac{\phi}{k\eta_w} \frac{\partial \theta_s}{\partial t} \frac{\partial S}{\partial \theta_s}. \end{aligned} \quad (\text{A2})$$

[64] In what follows I shall need to define the gradient vectors

$$\mathbf{p} = \nabla \theta_p \quad (\text{A3})$$

$$\mathbf{s} = \nabla \theta_s. \quad (\text{A4})$$

[65] From the particular form of the saturation and pressure, given by expansions (22) and (23), I note that to order  $\varepsilon^0$ ,

$$\frac{\partial S}{\partial \theta_s} = S_0 - S_b = \bar{S} \quad (\text{A5})$$

$$\frac{\partial P}{\partial \theta_p} = P_0 - P_b = \bar{P}. \quad (\text{A6})$$

[66] The quantities  $\bar{S}$  and  $\bar{P}$  signify the change in saturation and pressure from the background value to the value after the passage of the two-phase front. Incorporating all of these considerations into expression (A2) produces the more compact expression

$$\chi_w \mathbf{s} \cdot \mathbf{p} \bar{S} \bar{P} + p^2 \bar{P} - \rho_w \chi_w \mathbf{s} \cdot \mathbf{Z} \bar{S} = \frac{\alpha_T}{k\eta_w} \bar{S} \bar{P} \frac{\partial \theta_p}{\partial t} + \frac{\phi}{k\eta_w} \bar{S} \frac{\partial \theta_s}{\partial t}, \quad (\text{A7})$$

where  $p$  and  $s$  are the magnitudes of the pressure and saturation phase gradient vectors, respectively.

## A2. Second of the Governing Equations

[67] Now consider the second of the governing equations (15), expressing the differential operators in terms of the slow variables,

$$\begin{aligned} & \varepsilon \nabla \kappa \cdot \left( \varepsilon \nabla P + \nabla \theta_p \frac{\partial P}{\partial \theta_p} \right) \\ &+ \chi_n \left( \varepsilon \nabla S + \nabla \theta_s \frac{\partial S}{\partial \theta_s} \right) \cdot \left( \varepsilon \nabla P + \nabla \theta_p \frac{\partial P}{\partial \theta_p} \right) \\ &+ \varepsilon \nabla \cdot \left( \varepsilon \nabla P + \nabla \theta_p \frac{\partial P}{\partial \theta_p} \right) \\ &+ \nabla \theta_p \cdot \frac{\partial}{\partial \theta_p} \left( \varepsilon \nabla P + \nabla \theta_p \frac{\partial P}{\partial \theta_p} \right) \\ &- \rho_n \varepsilon \nabla \kappa \cdot \mathbf{Z} \\ &- \rho_n \chi_n \left( \varepsilon \nabla S + \nabla \theta_s \frac{\partial S}{\partial \theta_s} \right) \cdot \mathbf{Z} \\ &+ \varepsilon \gamma_c \nabla \kappa \cdot \left( \varepsilon \nabla S + \nabla \theta_s \frac{\partial S}{\partial \theta_s} \right) \\ &+ \Upsilon \left( \varepsilon \nabla S + \nabla \theta_s \frac{\partial S}{\partial \theta_s} \right) \cdot \left( \varepsilon \nabla S + \nabla \theta_s \frac{\partial S}{\partial \theta_s} \right) \\ &+ \varepsilon \gamma_c \nabla \cdot \left( \varepsilon \nabla S + \nabla \theta_s \frac{\partial S}{\partial \theta_s} \right) \end{aligned}$$

$$\begin{aligned} &+ \gamma_c \nabla \theta_s \cdot \frac{\partial}{\partial \theta_s} \left( \varepsilon \nabla S + \nabla \theta_s \frac{\partial S}{\partial \theta_s} \right) \\ &= \frac{\alpha_T}{k\eta_n} (1-S) \left( \varepsilon \frac{\partial P}{\partial T} + \frac{\partial \theta_p}{\partial t} \frac{\partial P}{\partial \theta_p} \right) \\ &- \frac{\phi}{k\eta_n} \left( \varepsilon \frac{\partial S}{\partial T} + \frac{\partial \theta_s}{\partial t} \frac{\partial S}{\partial \theta_s} \right). \end{aligned} \quad (\text{A8})$$

[68] To zeroth order in  $\varepsilon$  I obtain the following form for the second governing equation:

$$\begin{aligned} & \chi_n \nabla \theta_s \cdot \nabla \theta_p \frac{\partial S}{\partial \theta_s} \frac{\partial P}{\partial \theta_p} + \nabla \theta_p \cdot \nabla \theta_p \frac{\partial^2 P}{\partial \theta_p^2} - \rho_n \chi_n \nabla \theta_s \cdot \mathbf{Z} \frac{\partial S}{\partial \theta_s} \\ &+ \Upsilon \nabla \theta_s \cdot \nabla \theta_s \left( \frac{\partial S}{\partial \theta_s} \right)^2 + \gamma_c \nabla \theta_s \cdot \nabla \theta_s \frac{\partial^2 S}{\partial \theta_s^2} \\ &= \frac{\alpha_T}{k\eta_n} (1-S) \frac{\partial \theta_p}{\partial t} \frac{\partial P}{\partial \theta_p} - \frac{\phi}{k\eta_n} \frac{\partial \theta_s}{\partial t} \frac{\partial S}{\partial \theta_s}. \end{aligned} \quad (\text{A9})$$

[69] Making the substitutions discussed above (equations (A3) through (A6)), equation (A10) takes the form

$$\begin{aligned} & \chi_n \mathbf{s} \cdot \mathbf{p} \bar{S} \bar{P} + p^2 \bar{P} - \rho_n \chi_n \mathbf{s} \cdot \mathbf{Z} \bar{S} + \Upsilon \bar{S}^2 \bar{S}^2 + \gamma_c \bar{S}^2 \bar{S} \\ &= \frac{\alpha_T}{k\eta_n} (1-S) \bar{P} \frac{\partial \theta_p}{\partial t} - \frac{\phi}{k\eta_n} \bar{S} \frac{\partial \theta_s}{\partial t}. \end{aligned} \quad (\text{A10})$$

[70] Equations (A7) and (A10) form the starting point for the analysis in the main portion of this paper.

## Appendix B: Computation of the Phase for a Separable Function

[71] In this appendix I derive an explicit expression for the phase function  $\theta(\mathbf{x}, t)$ . In doing so I shall assume a separable form for the phase function

$$\theta(\mathbf{x}, t) = \beta(t) \sigma^2(\mathbf{x}) \quad (\text{B1})$$

and use the separation of variables to solve equation (42). Unfortunately, the gravitational term in equation (42) prevents one from separating the spatial and temporal variables. Therefore, I shall have to neglect gravitational effects, assuming that either the density contrast between the fluid phases is small or that the flow is dominantly horizontal, perpendicular to the gravitational field. In that case, equation (42) reduces to

$$\nabla \theta \cdot \nabla \theta - \Omega \frac{\partial \theta}{\partial t} = 0. \quad (\text{B2})$$

[72] Equation (B2), without gravity, is of sufficient interest and covers a number of important situations that it is worthy of consideration. Furthermore, I treat such problems in section 3, where I compare the asymptotic estimates of propagation time with estimates from a numerical simulator. Substituting the separable form (B1) into equation (B2) and noting that

$$\nabla \theta = 2\beta \sigma \nabla \sigma \quad (\text{B3})$$

$$\frac{\partial \theta}{\partial t} = \sigma^2 \frac{d\beta}{dt}, \quad (\text{B4})$$

where I have used the total derivative for  $\beta(t)$  because it only depends upon the single variable  $t$ , results in the expressions

$$4\beta^2\sigma^2\nabla\sigma\cdot\nabla\sigma - \Omega\sigma^2\frac{d\beta}{dt} = 0 \quad (\text{B5a})$$

or

$$\frac{\nabla\sigma\cdot\nabla\sigma}{\Omega} - \frac{1}{4\beta^2}\frac{d\beta}{dt} = 0. \quad (\text{B5b})$$

[73] Equations (B5a) and (B5b) are separable if  $\Omega$  is either separable or only depends upon  $\mathbf{x}$ . The time dependence of  $\Omega$  enters through the amplitude changes  $\bar{P}$  and  $\bar{S}$ , which multiply each factor. The amplitude changes may not be functions of time. For example, the change in saturation because of the passage of the front is primarily determined by the preexisting saturation and by the properties of the relative permeability curves describing the material. Thus, the saturation change  $\bar{S}$  is essentially a function of position and does not change significantly as a function of time. That is, the saturation change will be the same, no matter when the two-phase front passes through a particular region. Alternatively, during the initiation of injection, a transient pressure change can propagate away from the injection well, accompanied by a very small change in saturation. Thus, the saturation change that occurs because of the passage of the front  $\bar{S}$  is negligible, and only the terms associated with  $\bar{P}$  are significant. Then the terms  $\bar{P}$  will factor out of  $\Omega$ , and the time-dependent terms will cancel.

[74] For situations in which  $\Omega$  only depends upon  $\mathbf{x}$ , equations (B5a) and (B5b), written as

$$\frac{\nabla\sigma\cdot\nabla\sigma}{\Omega} = \frac{1}{4\beta^2}\frac{d\beta}{dt}, \quad (\text{B6})$$

expresses the equality of the left-hand side, which only depends upon spatial coordinates  $\mathbf{x}$ , and the right-hand side, which only depends upon time  $t$ . This means that the terms on either side must equal a constant value, which I denote by  $C$ . Thus, for the right-hand side of equation (B6),

$$\frac{1}{4\beta^2}\frac{d\beta}{dt} = C \quad (\text{B7})$$

or

$$\beta = -\frac{1}{4Ct}. \quad (\text{B8})$$

[75] Similarly, the left-hand side of equation (B6) produces the partial differential equation

$$\nabla\sigma\cdot\nabla\sigma = C\Omega \quad (\text{B9})$$

known as the eikonal equation [Kravtsov and Orlov, 1990]. A solution of the eikonal equation follows from an application of the method of characteristics [Courant and Hilbert, 1962, p. 97]. The characteristic equations associated with

equation (B9) follow if I define the Hamiltonian function  $F(\mathbf{x}, \mathbf{p})$  as

$$F(\mathbf{x}, \mathbf{p}) = \mathbf{p}\cdot\mathbf{p} - C\Omega, \quad (\text{B10})$$

with equation (B9) given by  $F(\mathbf{x}, \mathbf{p}) = 0$ . As noted by Courant and Hilbert [1962, p. 97], the characteristic equations are a pair of ordinary differential equations:

$$\frac{dx_i}{ds} = \frac{\partial F}{\partial p_i} \quad (\text{B11})$$

$$\frac{dp_i}{ds} = -\frac{\partial F}{\partial x_i} \quad (\text{B12})$$

or, making use of the Hamiltonian function in equation (B10),

$$\frac{d\mathbf{x}}{ds} = 2\mathbf{p} \quad (\text{B13})$$

$$\frac{d\mathbf{p}}{ds} = C\nabla\Omega. \quad (\text{B14})$$

[76] Equation (B13) defines a trajectory  $\mathbf{x}(s)$  over which a solution is constructed. The variable  $s$  is the distance along the trajectory. Using the trajectory to define a coordinate system, I can rewrite the eikonal equation (B9), noting that  $\mathbf{p}$  is tangent to the trajectory  $\mathbf{x}(s)$ :

$$\frac{d\sigma}{ds} = \sqrt{C\Omega}. \quad (\text{B15})$$

[77] Integrating along the trajectory, I arrive at an expression for  $\sigma(\mathbf{x})$ :

$$\sigma[\mathbf{x}(s)] = \sqrt{C} \int_{\mathbf{x}(s)} \sqrt{\Omega} ds. \quad (\text{B16})$$

[78] Combining the functions (B8) for  $\beta(t)$  and (B16) for  $\sigma(\mathbf{x})$  produces an expression for the phase  $\theta(\mathbf{x}, t)$  (see equation (B1)),

$$\theta[\mathbf{x}(s), t] = -\frac{1}{4t} \left( \int_{\mathbf{x}(s)} \sqrt{\Omega} ds \right)^2. \quad (\text{B17})$$

### Appendix C: An Interpretation of the Phase Function

[79] If the amplitude functions  $S_0(\mathbf{X}, T)$  and  $P_0(\mathbf{X}, T)$  vary monotonically as functions of time, then the derivatives (53) and (54) should display single peaks, associated with the peak of each Gaussian function. I can derive equations for the peaks by differentiating (53) and (54) and setting the result to zero. For example, differentiating (53) with respect to time,

$$\frac{\partial^2 \bar{S}}{\partial t^2} = e^{\theta_s} \left[ S_0 \frac{\partial \theta_s}{\partial t} + \frac{\partial S_0}{\partial t} \right]. \quad (\text{C1})$$

[80] The exponential term in (C1) is nonzero as long as one stays away from the origin. Thus, factoring out the

exponential term, the condition for the peak of the time derivative of  $\bar{S}$  is

$$S_0 \frac{\partial \theta_s}{\partial t} + \frac{\partial S_0}{\partial t} = 0. \quad (\text{C2})$$

[81] In order to derive a specific expression relating the phase to the peak of the time derivative of the saturation, I shall need to introduce additional assumptions. Here I consider one possible form for the amplitude function  $S_0(\mathbf{X}, t)$ , a power law time dependence. Other amplitude functions, such as a form based upon Hermite polynomials, are possible. Motivated by the solution to the linear diffusion equation [Vasco *et al.*, 2000], I consider the specific form

$$S_0(\mathbf{X}, t) = t^{-\alpha_s} S_x(\mathbf{X}), \quad (\text{C3})$$

where  $\alpha_s$  is constant and  $S_x(\mathbf{X})$  is a function of  $\mathbf{X}$ . Thus, for an amplitude function of the form (C3), equation (C2) becomes

$$t^{-\alpha_s} \frac{\partial \theta_s}{\partial t} - \alpha_s t^{-\alpha_s - 1} = 0. \quad (\text{C4})$$

[82] Third, I assume that the phase function  $\theta_s(\mathbf{X}, t)$  can be written in the separable form,  $\theta(\mathbf{x}, t) = \beta(t)\sigma^2(\mathbf{x})$ , as derived in Appendix B. With these three assumptions, equation (C4) reduces to

$$\frac{\sigma^2}{4} - \alpha_s t = 0. \quad (\text{C5})$$

[83] I can relate the phase component  $\sigma(\mathbf{X})$  to the time at which the time derivative of the saturation is a maximum or minimum. I denote the time at which the derivative is a peak as  $T_{\text{peak}}$ . The specific relationship is

$$\sigma = 2\sqrt{\alpha_s T_{\text{peak}}}, \quad (\text{C6})$$

or, solving for  $T_{\text{peak}}$  and using the definition of  $\sigma$  given by (B16),

$$\sqrt{T_{\text{peak}}} = \frac{1}{2\sqrt{\alpha_s}} \int_{\mathbf{x}(s)} \sqrt{\Omega} ds. \quad (\text{C7})$$

[84] Thus, under the stated assumptions, the time derivative of the saturation is a maximum at the time  $T_{\text{peak}}$ , and this time is determined by the medium parameters, as contained in  $\Omega$  (see equation (40)). A similar analysis can be applied to the pressure variation, under the corresponding assumption that the pressure amplitude has the separable form

$$P_0(\mathbf{X}, t) = t^{-\alpha_p} P_x(\mathbf{X}), \quad (\text{C8})$$

where  $P_x(\mathbf{X})$  is the spatial component of the pressure amplitude function. The resulting peak time for the pressure time derivative is

$$\sqrt{T_{\text{peak}}} = \frac{1}{2\sqrt{\alpha_p}} \int_{\mathbf{x}(s)} \sqrt{\Omega} ds, \quad (\text{C9})$$

which is similar to the expression for the linear diffusion equation [Vasco *et al.*, 2000].

[85] **Acknowledgments.** This work was supported by the Assistant Secretary, Office of Basic Energy Sciences of the U. S. Department of Energy under contract DE-AC02-05CH11231.

## References

- Anile, A. M., J. K. Hunter, P. Pantano, and G. Russo (1993), *Ray Methods for Nonlinear Waves in Fluids and Plasmas*, Longman, New York.
- Arridge, S. (1999), Optical tomography in medical imaging, *Inverse Probl.*, 15, R41–R93.
- Bear, J. (1972), *Dynamics of Fluids in Porous Media*, Dover, New York.
- Bell, J. W., F. Amelung, A. Ferretti, M. Bianchi, and F. Novali (2008), Permanent scatterer InSAR reveals seasonal and long-term aquifer-system response to groundwater pumping and artificial recharge, *Water Resour. Res.*, 44, W02407, doi:10.1029/2007WR006152.
- Brauchler, R., R. Liedl, and P. Dietrich (2003), A travel time based hydraulic tomographic approach, *Water Resour. Res.*, 39(12), 1370, doi:10.1029/2003WR002262.
- Brooks, R. H., and A. T. Corey (1966), Properties of porous media affecting fluid flow, *Proc. Am. Soc. Civ. Eng.*, 92, 61–87.
- Butler, J. J., C. D. McElwee, and G. C. Bohling (1999), Pumping tests in networks of multilevel sampling wells: Motivation and methodology, *Water Resour. Res.*, 35(11), 3553–3560, doi:10.1029/1999WR900231.
- Cerveny, V. (1972), Seismic rays and ray intensities in inhomogeneous anisotropic media—I. Theory, *Geophys. J. R. Astron. Soc.*, 29, 1–13.
- Chapman, C. H., and R. G. Pratt (1992), Traveltime tomography in anisotropic media—I. Theory, *Geophys. J. Int.*, 109, 1–19.
- Cheng, H., Z. He, and A. Datta-Gupta (2005), A comparison of travel-time and amplitude matching for field-scale production data integration: Sensitivity, non-linearity, and practical implications, *SPE J.*, 10, 75–90.
- Cohen, J. K., and R. M. Lewis (1967), A ray method for the asymptotic solution of the diffusion equation, *J. Inst. Maths Applics.*, 3, 266–290.
- Corey, A. T. (1954), The interrelation between gas and oil relative permeabilities, *Prod. Mon.*, 19, 38–41.
- Courant, R., and D. Hilbert (1962), *Methods of Mathematical Physics*, Interscience, New York.
- Cox, D., J. Little, and D. O'Shea (1998), *Using Algebraic Geometry*, Springer, New York.
- Crandall, M. G., and P.-L. Lions (1983), Viscosity solutions of Hamilton-Jacobi equations, *Trans. Am. Math. Soc.*, 277, 1–43.
- Crandall, M. G., L. C. Evans, and P.-L. Lions (1984), Some properties of viscosity solutions of Hamilton-Jacobi equations, *Trans. Am. Math. Soc.*, 282, 487–502.
- Datta-Gupta, A., and M. King (1995), A semianalytical approach to tracer flow modeling in heterogeneous permeable media, *Adv. Water Resour.*, 18, 9–24.
- Datta-Gupta, A., S. Yoon, D. W. Vasco, and G. A. Pope (2002), Inverse modeling of partitioning interwell tracer tests: A streamline approach, *Water Resour. Res.*, 38(6), 1079, doi:10.1029/2001WR000597.
- de Marsily, G. (1986), *Quantitative Hydrogeology*, Academic, San Diego, Calif.
- Eaton, D. W. S. (1993), Finite difference travel-time calculation for anisotropic media, *Geophys. J. Int.*, 114, 273–280.
- Fatt, I., and W. A. Klikoff (1959), Effect of fractional wettability on multiphase flow through porous media, *Trans. Am. Inst. Min. Metall. Eng.*, 216, 246–250.
- Hsieh, P. A., S. P. Neuman, G. K. Stiles, and E. S. Simpson (1985), Field determination of the three-dimensional hydraulic conductivity tensor of anisotropic media: 2. Methodology and application to fractured rocks, *Water Resour. Res.*, 21(11), 1667–1676, doi:10.1029/WR021i011p01667.
- Iyer, H. M., and K. Hirahara (1993), *Seismic Tomography: Theory and Practice*, Chapman and Hall, London.
- Karal, F. C., and J. B. Keller (1959), Elastic wave propagation in homogeneous and inhomogeneous media, *J. Acoust. Soc. Am.*, 31, 694–705.
- Karasaki, K., B. Freifeld, A. Cohen, K. Grossenbacher, P. Cook, and D. Vasco, (2000), A multi-disciplinary fractured rock characterization study at the Raymond field site, Raymond, CA, *J. Hydrol.*, 236, 17–34.
- Kline, M., and I. W. Kay (1965), *Electromagnetic Theory and Geometrical Optics*, John Wiley, New York.
- Kowalsky, M. B., S. Finsterle, and Y. Rubin (2004), Estimating flow parameter distributions using ground-penetrating radar and hydrological

- measurements during transient flow in the vadose zone, *Adv. Water Resour.*, 27, 583–599.
- Kowalsky, M. B., S. Finsterle, J. Peterson, S. Hubbard, Y. Rubin, E. Majer, A. Ward, and G. Gee (2005), Estimation of field-scale soil hydraulic and dielectric parameters through joint inversion of GPR and hydrological data, *Water Resour. Res.*, 41, W11425, doi:10.1029/2005WR004237.
- Kravtsov, Y. A., and Y. I. Orlov (1990), *Geometrical Optics of Inhomogeneous Media*, Springer, Berlin.
- Lanczos, C. (1986), *The Variational Principles of Mechanics*, Dover, New York.
- Lecomte, I. (1993), Finite difference calculation of first traveltimes in anisotropic media, *Geophys. J. Int.*, 113, 318–342.
- Lunenburg, R. K. (1966), *Mathematical Theory of Optics*, Univ. of Calif. Press, Berkeley.
- Maslov, V. P., and G. A. Omel'yanov (2001), *Geometric Asymptotics for Nonlinear PDE*, Am. Math. Soc., Providence, R. I.
- Mualem, Y. (1976), A new model for predicting the hydraulic conductivity of unsaturated porous media, *Water Resour. Res.*, 12(3), 513–522, doi:10.1029/WR012i003p00513.
- Noble, B., and J. W. Daniel (1977), *Applied Linear Algebra*, Prentice Hall, Englewood Cliffs, N. J.
- Paillet, F. L. (1993), Using borehole geophysics and cross-borehole flow testing to define connections between fracture zones in bedrock aquifers, *J. Appl. Geophys.*, 30, 261–279.
- Peaceman, D. W. (1977), *Fundamentals of Numerical Reservoir Simulation*, Elsevier Sci., Amsterdam.
- Press, W. H., S. A. Teukolsky, W. T. Vetterling, and B. P. Flannery (1992), *Numerical Recipes*, Cambridge Univ. Press, Cambridge, U. K..
- Pruess, K., C. Oldenburg, and G. Moridis (1999), TOUGH2 user's guide, version 2.0, *Rep. LBNL 43134*, Lawrence Berkeley Natl. Lab., Berkeley, Calif.
- Qian, J., and W. W. Symes (2001), Paraxial eikonal solvers for anisotropic quasi-P travel times, *J. Comput. Phys.*, 173, 256–278.
- Rucci, A., D. W. Vasco, and F. Novali (2010), Fluid pressure arrival time tomography: Estimation and assessment in the presence of inequality constraints, with an application to a producing gas field at Krechba, Algeria, *Geophysics*, 75, O39–O55.
- Schmidt, D. A., and R. Bürgmann (2003), Time-dependent land uplift and subsidence in the Santa Clara valley, California, from a large interferometric synthetic aperture radar data set, *J. Geophys. Res.*, 108(B9), 2416, doi:10.1029/2002JB002267.
- Sethian, J. A. (1990), Numerical algorithms for propagating interfaces: Hamilton-Jacobi equations and conservation laws, *J. Differ. Geom.*, 31, 131–161.
- Sethian, J. A. (1999), *Level Set Methods*, Cambridge Univ. Press, Cambridge, U. K..
- Sethian, J. A., and J. D. Strain (1992), Crystal growth and dendritic solidification, *J. Comput. Phys.*, 98, 231–253.
- Shen, M. C., (1983), Ray method for flow of a compressible viscous fluid, *SIAM J. Appl. Math.*, 43, 822–833.
- Sneddon, I. N. (2006), *Elements of Partial Differential Equations*, Dover, New York.
- Soukina, S. M., D. Gajewski, and B. M. Kashtan (2003), Traveltime computation for 3D anisotropic media by a finite-difference perturbation method, *Geophys. Prospect.*, 51, 431–441.
- Sturmfels, B. (2002), *Solving Systems of Polynomial Equations*, Am. Math. Soc., Providence, R. I.
- Sun, N.-Z. (1994), *Inverse Problems in Groundwater Modeling*, Kluwer Acad., Norwell, Mass.
- Tuncay, K., and M. Corapcioglu (1996), Body waves in poroelastic media saturated by two immiscible fluids, *J. Geophys. Res.*, 101(B11), 25,149–25,159, doi:10.1029/96JB02297.
- van Genuchten, M. T. (1980), A closed-form equation for predicting the hydraulic conductivity of unsaturated soils, *Soil Sci. Soc. Am. J.*, 44, 892–898.
- van Trier, J., and W. W. Symes (1991), Upwind finite-difference calculations of traveltimes, *Geophysics*, 56, 812–821.
- Vasco, D. W. (2004a), An asymptotic solution for two-phase flow in the presence of capillary forces, *Water Resour. Res.*, 40, W12407, doi:10.1029/2003WR002587.
- Vasco, D. W. (2004b), Seismic imaging of reservoir flow properties: Time-lapse pressure changes, *Geophysics*, 69, 511–521.
- Vasco, D. W. (2008a), Zeroth-order inversion of transient pressure observations, *Inverse Probl.*, 24, 1–21, doi:10.1088/0266-5611/24/2/025013.
- Vasco, D. W. (2008b), Trajectory-based methods for modeling and characterization, in *Quantitative Information Fusion for Hydrological Sciences*, *Stud. Comput. Intell.*, vol. 79, edited by X. Cai and T.-C. J. Yeh, pp. 69–103, Springer, Berlin.
- Vasco, D. W. (2010), On fluid flow in a heterogeneous medium under non-isothermal conditions, *Water Resour. Res.*, 46, W12513, doi:10.1029/2010WR009571.
- Vasco, D. W., and A. Datta-Gupta (1999), Asymptotic solutions for solute transport: A formalism for tracer tomography, *Water Resour. Res.*, 35(1), 1–16, doi:10.1029/98WR02742.
- Vasco, D. W., and S. Finsterle (2004), Numerical trajectory calculations for the efficient inversion of flow and tracer observations, *Water Resour. Res.*, 40, W01507, doi:10.1029/2003WR002362.
- Vasco, D. W., S. Yoon, and A. Datta-Gupta (1999), Integrating dynamic data into high-resolution reservoir models using streamline-based analytic sensitivity coefficients, *SPE J.*, 4, 389–399.
- Vasco, D. W., H. Keers, and K. Karasaki (2000), Estimation of reservoir properties using transient pressure data: An asymptotic approach, *Water Resour. Res.*, 36(12), 3447–3465, doi:10.1029/2000WR900179.
- Vasco, D. W., A. Datta-Gupta, R. Behrens, P. Condon, and J. Rickett (2004), Seismic imaging of reservoir flow properties: Time-lapse amplitude changes, *Geophysics*, 69, 1425–1442.
- Vasco, D. W., A. Rucci, A. Ferretti, F. Novali, R. C. Bissell, P. S. Ringrose, A. S. Mathieson, and I. W. Wright (2010), Satellite-based measurements of surface deformation reveal fluid flow associated with the geological storage of carbon dioxide, *Geophys. Res. Lett.*, 37, L03303, doi:10.1029/2009GL041544.
- Vesselinov, V. V., S. P. Neuman, and W. A. Illman (2001), Three-dimensional numerical inversion of pneumatic cross-hole tests in unsaturated fractured tuff: 2. Equivalent parameters, high-resolution stochastic imaging, and scale effects, *Water Resour. Res.*, 37(12), 3019–3041, doi:10.1029/2000WR000135.
- Vidale, J. (1988), Finite-difference calculation of travel times, *Bull. Seismol. Soc. Am.*, 78, 2062–2076.
- Virieux, J., C. Flores-Luna, and D. Gibert (1994), Asymptotic theory for diffusive electromagnetic imaging, *Geophys. J. Int.*, 119, 857–868.
- Whitham, G. B. (1974), *Linear and Nonlinear Waves*, John Wiley, New York.
- Yeh, T. C., and S. Liu (2000), Hydraulic tomography: Development of a new aquifer test method, *Water Resour. Res.*, 36(8), 2095–2105, doi:10.1029/2000WR900114.

D. W. Vasco, Earth Sciences Division, Lawrence Berkeley National Laboratory, Building 90, 1 Cyclotron Road, Berkeley, CA 94720, USA. (dvwasco@lbl.gov)